

# Performance of internal Covariance Estimators for Cosmic Shear Correlation Functions

O. Friedrich<sup>1,2\*</sup>, S. Seitz<sup>1,2</sup>, T. F. Eifler<sup>3,4</sup>, D. Gruen<sup>1,2</sup>

<sup>1</sup>University Observatory Munich, Scheinerstrasse 1, 81679 Munich, Germany

<sup>2</sup>Max Planck Institute for Extraterrestrial Physics, Giessenbachstrasse, 85748 Garching, Germany

<sup>3</sup>Jet Propulsion Laboratory, California Institute of Technology, 4800 Oak Grove Dr., Pasadena, CA 91109

<sup>4</sup>California Institute of Technology, Pasadena, CA 91125, USA

23 July 2018

## ABSTRACT

Data re-sampling methods such as the delete-one jackknife are a common tool for estimating the covariance of large scale structure probes. In this paper we investigate the concepts of internal covariance estimation in the context of cosmic shear two-point statistics. We demonstrate how to use log-normal simulations of the convergence field and the corresponding shear field to carry out realistic tests of internal covariance estimators and find that most estimators such as jackknife or sub-sample covariance can reach a satisfactory compromise between bias and variance of the estimated covariance.

In a forecast for the complete, 5-year DES survey we show that internally estimated covariance matrices can provide a large fraction of the true uncertainties on cosmological parameters in a 2D cosmic shear analysis. The volume inside contours of constant likelihood in the  $\Omega_m$ - $\sigma_8$  plane as measured with internally estimated covariance matrices is on average  $\gtrsim 85\%$  of the volume derived from the true covariance matrix. The uncertainty on the parameter combination  $\Sigma_8 \sim \sigma_8 \Omega_m^{0.5}$  derived from internally estimated covariances is  $\sim 90\%$  of the true uncertainty.

**Key words:** large scale structure – cosmic shear – covariance – jackknife – angular correlation function

## 1 INTRODUCTION

Two-point statistics of cosmological random fields such as the cosmic shear correlation functions or the galaxy clustering angular correlation function are common probes of the large scale structure of the universe. Recent measurements of these correlation functions are e.g. reported in Thomas et al. (2011); Kilbinger et al. (2013); de Simoni et al. (2013); Becker et al. (2015). In order to use these statistics for constraining cosmological models one needs a quantitative description of the joint distribution of the correlation function estimators. When assuming multivariate Gaussian errors, this is given by the covariance matrix. On large angular scales this covariance matrix can - both for cosmic shear and galaxy clustering - be well described by a Gaussian approximation for the involved fields (Schneider et al. 2002; Crocce et al. 2011). It has, however, been shown, that the Gaussian approximation fails to describe the true PDF of the weak lensing convergence field (Taruya et al. 2002;

Vale & White 2003) and that it underestimates the true covariance of the cosmic shear correlation functions on small scales, which can be alleviated by an empirical re-scaling (Semboloni et al. 2007; Sato et al. 2011), a log-normal approximation (Hilbert et al. 2011), or halo model approaches (e.g. Cooray & Hu 2001; Takada & Jain 2009; Eifler et al. 2014).

Alternatives to modelling the covariance matrix are to estimate it from many independent realisations of cosmological N-body simulations or to estimate it internally, i.e. from the data itself. The latter method is independent of assuming a particular cosmological model and is hence often used to complement the other methods (Kilbinger et al. 2013; Wang et al. 2013; Becker et al. 2015.).

So far the performance of internal covariance estimators has only been systematically studied for the galaxy clustering 2-pt function (in most detail by Norberg et al. 2009) or for cross-correlations of the Cosmic Microwave Background (CMB) and the galaxy field (Cabr e et al. 2007). In our paper, we will concentrate on cosmic shear correlation functions. We will show that the shape noise part of the covari-

\* E-mail: oliverf@usm.uni-muenchen.de

ance can be very accurately estimated internally while the cosmic variance part is generally underestimated. Gaussian simulations of the convergence field hence yield an overly optimistic test of internal covariance estimators, since the Gaussian model underpredicts the cosmic variance contribution to the covariance. We overcome this problem by employing log-normal simulations of the convergence field.

In our paper we want to study the performance of internal covariance estimators such as bootstrap, jackknife or the sub-sample covariance. There is no complete agreement in the literature yet on whether internal covariance estimates can be used to constrain cosmological parameters from measured 2pt-correlations or whether they are a mere tool to generate reasonable errorbars in plots of correlation functions (see e.g. Norberg et al. 2009; Wang et al. 2013; de Simoni et al. 2013; Taylor et al. 2013). We want to address the questions of how many internal resamplings are required in order to get a stable covariance matrix, whether internal estimators over- or underestimate the covariance matrix and whether/how internal covariance estimates can yield unbiased estimates of the *inverse* covariance matrix.

Our paper is organized as follows: In section 2 we introduce the cosmic shear correlation functions and explain the Gaussian and the log-normal model for the covariance of 2-pt. function estimators. In section 3 we describe the simulations we use to generate mock shape catalogues that follow any given input power spectrum and whose underlying convergence field has a log-normal PDF. These are the simulations with which we will test the performance of internal covariance estimators.

In section 4 we introduce two principle ways of performing jackknife estimation of the covariance of two-point measures - the pair-jackknife and the galaxy-jackknife. Furthermore, we are explaining why jackknife, bootstrap and subsample covariance are almost equivalent.

In section 5 we apply internal covariance estimation to simulated cosmic shear surveys. We show that in the pair-scheme all estimators are almost identical and we demonstrate the systematic effects of the different estimation schemes when varying the number of re-samplings. Our method to find optimal estimation schemes has to be re-run for any specific survey, because the performance of internal estimators depends crucially on the depth and area of a survey. In the end of section 5 we configure our simulations to match the complete, 5-year Dark Energy Survey (DES, The Dark Energy Survey Collaboration 2005; Flaugher 2005) and test the accuracy of jackknife covariance matrices for this particular setting. The code used for our simulations is made publicly available<sup>1</sup>.

In section 6 we discuss the results of our work.

## 2 COSMIC SHEAR BASICS

### 2.1 Cosmic Shear Correlation Functions

Cosmic shear measures the correlated distortion of galaxy shapes due to gravitational lensing by the large scale structure of the universe as a function of the angular distance of galaxy pairs on the sky. We follow here the notation of Schneider et al. (2002) and employ the flat-sky-approximation, i.e. we assume a tangential Cartesian coordinate system  $\boldsymbol{\vartheta} = (\vartheta_1, \vartheta_2)$  on the sky.

In this coordinate system the cosmic shear field is at each point characterized by a complex number  $\gamma(\boldsymbol{\vartheta}) = \gamma_1 + i\gamma_2$ . If the separation vector  $\Delta\boldsymbol{\vartheta} = \boldsymbol{\vartheta}_2 - \boldsymbol{\vartheta}_1$  of two points on the sky has the polar angle  $\phi$  then the *tangential* and *cross* components of  $\gamma$  at  $\boldsymbol{\vartheta}_2$  and  $\boldsymbol{\vartheta}_1$  (with respect to each other) are defined as

$$\gamma_t = -\mathcal{R}e\left(\gamma e^{-2i\phi}\right) \quad ; \quad \gamma_\times = -\mathcal{I}m\left(\gamma e^{-2i\phi}\right). \quad (1)$$

The *cosmic shear correlation functions*  $\xi_\pm(\theta)$  are defined as the expectation values

$$\xi_\pm(\theta) = \langle \gamma_{t,1} \gamma_{t,2} \rangle \pm \langle \gamma_{\times,1} \gamma_{\times,2} \rangle, \quad (2)$$

where  $\theta$  is the absolute value of  $\Delta\boldsymbol{\vartheta}$ . It can be computed in terms of the power spectrum  $P_\kappa(\ell)$  of the scalar *convergence field*  $\kappa(\boldsymbol{\vartheta})$  as

$$\xi_\pm(\theta) = \frac{1}{2\pi} \int d\ell \ell P_\kappa(\ell) J_{0,4}(\ell\theta), \quad (3)$$

where  $J_0(x)$  ( $J_4(x)$ ) is the 0-th order (4-th order) Bessel function.

The shape of a galaxy can be characterized by a complex number  $\epsilon$  which is to first order the sum of the intrinsic shape  $\epsilon^s$  of the galaxy and the distortion caused by gravitational lensing, i.e. the value  $\gamma(\boldsymbol{\vartheta})$  at the location  $\boldsymbol{\vartheta}$  of the galaxy,

$$\epsilon = \epsilon^s + \gamma. \quad (4)$$

In a cosmic shear survey the shapes  $\epsilon_i$  of many galaxies are measured and (cf. Schneider et al. 2002) an estimator for the correlation function can be constructed as

$$\hat{\xi}_\pm(\theta) = \frac{\sum_{ij} w_j w_j (\epsilon_{t,i} \epsilon_{t,j} \pm \epsilon_{\times,i} \epsilon_{\times,j}) \Delta_\theta(ij)}{\sum_{ij} w_j w_j \Delta_\theta(ij)}, \quad (5)$$

where we have allowed for some weighting scheme  $w_i$  for the shape measurements and where the filter  $\Delta_\theta(ij)$  selects all galaxy pairs  $(i, j)$  in the survey whose angular separation lies in some finite bin around  $\theta$ . The normalization in equation 5 is the effective number of galaxy pairs in a bin around  $\theta$ , which we will abbreviate as

$$N_p(\theta) = \sum_{ij} w_j w_j \Delta_\theta(ij). \quad (6)$$

### 2.2 Covariance of the Correlation Functions

The covariance matrix of the estimator in equation 5 is defined as

$$\begin{aligned} C_{\pm,\pm}(\theta_1, \theta_2) &= \langle (\hat{\xi}_\pm(\theta_1) - \xi_\pm(\theta_1)) (\hat{\xi}_\pm(\theta_2) - \xi_\pm(\theta_2)) \rangle \\ &= \langle \hat{\xi}_\pm(\theta_1) \hat{\xi}_\pm(\theta_2) \rangle - \xi_\pm(\theta_1) \xi_\pm(\theta_2). \end{aligned} \quad (7)$$

<sup>1</sup> [www.usm.uni-muenchen.de/people/oliverf/](http://www.usm.uni-muenchen.de/people/oliverf/), the code also contains many other useful features, that e.g. enable the user to create mock data suitable for galaxy-galaxy lensing or galaxy clustering measurements.

In order to compute this covariance matrix it is convenient to split  $\xi_{\pm}(\theta)$  into the three different contribution

$$\begin{aligned}\hat{\xi}_{\pm}^{nn}(\theta) &= \frac{\sum_{ij} w_i w_j (\epsilon_{t,i}^s \epsilon_{t,j}^s \pm \epsilon_{\times,i}^s \epsilon_{\times,j}^s) \Delta_{\theta}(ij)}{N_p(\theta)}, \\ \hat{\xi}_{\pm}^{ss}(\theta) &= \frac{\sum_{ij} w_i w_j (\gamma_{t,i} \gamma_{t,j} \pm \gamma_{\times,i} \gamma_{\times,j}) \Delta_{\theta}(ij)}{N_p(\theta)}, \\ \hat{\xi}_{\pm}^{sn}(\theta) &= \frac{\sum_{ij} w_i w_j (\epsilon_{t,i}^s \gamma_{t,j} \pm \epsilon_{\times,i}^s \gamma_{\times,j}) \Delta_{\theta}(ij)}{N_p(\theta)}\end{aligned}\quad (8)$$

which are the autocorrelation of the intrinsic shape noise, the autocorrelation of the shear signal and their cross correlation. The whole estimator 5 is given in terms of these as

$$\hat{\xi}_{\pm}(\theta) = \hat{\xi}_{\pm}^{nn}(\theta) + \hat{\xi}_{\pm}^{ss}(\theta) + 2 \cdot \hat{\xi}_{\pm}^{sn}(\theta).$$

Under the assumption that the shear signal and the shape noise are independent of each other it is obvious that

$$\langle \hat{\xi}_{\pm}^{nn}(\theta_1) \hat{\xi}_{\pm}^{sn}(\theta_2) \rangle = 0 = \langle \hat{\xi}_{\pm}^{ss}(\theta_1) \hat{\xi}_{\pm}^{sn}(\theta_2) \rangle.$$

If the intrinsic shape of any two galaxies is assumed to be uncorrelated, we can also conclude that

$$\langle \hat{\xi}_{\pm}^{nn} \rangle = 0 \text{ for } \theta > 0 \quad (9)$$

and hence

$$\langle \hat{\xi}_{\pm}^{nn}(\theta_1) \hat{\xi}_{\pm}^{ss}(\theta_2) \rangle = \langle \hat{\xi}_{\pm}^{nn}(\theta_1) \rangle \cdot \langle \hat{\xi}_{\pm}^{ss}(\theta_2) \rangle = 0 \text{ for } \theta_1, \theta_2 > 0.$$

The covariance matrix can thus be split into three different contributions,

$$C_{\pm,\pm} = C_{\pm,\pm}^{nn} + C_{\pm,\pm}^{ss} + C_{\pm,\pm}^{sn}, \quad (10)$$

namely

$$\begin{aligned}C_{\pm,\pm}^{nn}(\theta_1, \theta_2) &= \langle \hat{\xi}_{\pm}^{nn}(\theta_1) \hat{\xi}_{\pm}^{nn}(\theta_2) \rangle, \\ C_{\pm,\pm}^{ss}(\theta_1, \theta_2) &= \langle \hat{\xi}_{\pm}^{ss}(\theta_1) \hat{\xi}_{\pm}^{ss}(\theta_2) \rangle - \xi_{\pm}(\theta_1) \xi_{\pm}(\theta_2), \\ C_{\pm,\pm}^{sn}(\theta_1, \theta_2) &= 4 \cdot \langle \hat{\xi}_{\pm}^{sn}(\theta_1) \hat{\xi}_{\pm}^{sn}(\theta_2) \rangle.\end{aligned}\quad (11)$$

The  $C_{\pm,\pm}^{ss}$  term depends on 4-point functions of the shear field and is called the *cosmic variance* term. In order to evaluate it, further assumptions on the probability distribution function (PDF) of the shear or the convergence field are needed and we will discuss two possible models for the convergence PDF in sections 2.2.1 and 2.2.2 - the Gaussian and the log-normal model.

The contributions  $C_{\pm,\pm}^{nn}$  and  $C_{\pm,\pm}^{sn}$  can be computed without additional assumptions. In Joachimi et al. (2008) it is derived that they are given by<sup>2</sup>

$$\begin{aligned}C_{\pm,\pm}^{sn}(\theta_1, \theta_2) &= \frac{\sigma_{\epsilon}^2}{\pi A \bar{n}} \int d\ell \ell J_{0/4}(\ell\theta_1) J_{0/4}(\ell\theta_2) P_{\kappa}(\ell), \\ C_{++}^{nn}(\theta_1, \theta_2) &= C_{--}^{nn}(\theta_1, \theta_2) \\ &= \frac{\sigma_{\epsilon}^4}{N_p(\theta_1)} \cdot \delta_{\theta_1, \theta_2}, \\ C_{+-}^{nn}(\theta_1, \theta_2) &= 0,\end{aligned}\quad (12)$$

where  $A$  is the survey area,  $\bar{n}$  is the number density of galaxies,  $\sigma_{\epsilon}$  is the dispersion of the intrinsic ellipticity which is defined as

$$\sigma_{\epsilon}^2 := \langle \epsilon^s \epsilon^{s*} \rangle, \quad (13)$$

<sup>2</sup> as in Schneider et al. (2002) they employ an ensemble average over the galaxy positions to derive their expressions.

and  $P_{\kappa}$  is again the convergence power spectrum.

### 2.2.1 Gaussian Approximation

In the paper series by Schneider et al. (2002), Kilbinger & Schneider (2004) and Joachimi et al. (2008) the covariance matrix is studied in the Gaussian approximation, i.e. assuming that the convergence field has a Gaussian PDF such that its 4-point correlation functions can be expressed in terms of its 2-point correlation functions.

For the case where the survey geometry is much larger than the angular scales considered in the correlation functions, Joachimi et al. (2008) derive the following expressions for the cosmic variance term:

$$C_{\pm,\pm}^{ss}(\theta_1, \theta_2) = \frac{1}{\pi A} \int d\ell \ell J_{0/4}(\ell\theta_1) J_{0/4}(\ell\theta_2) P_{\kappa}^2(\ell). \quad (14)$$

However, due to the finite geometry of any given survey equation 14 generally overestimates the covariance of Gaussian field as was demonstrated in Sato et al. (2011). This *finite area effect* according to Sato et al. is not important for surveys larger than 1000 deg<sup>2</sup>. For smaller surveys a method developed in Kilbinger & Schneider (2004) which doesn't employ an ensemble average over galaxy positions should be used to evaluate the Gaussian covariance. This method was for example used in the analysis of CHFTLenS data in Kilbinger et al. (2013). The finite area effect is also important for internal covariance estimation and will be further discussed in section 4.4.

### 2.2.2 Shifted Log-Normal Approximation

As e.g. reported by Taruya et al. (2002), Vale & White (2003) or by Hilbert et al. (2011) the Gaussian model fails to describe the true PDF of the convergence and especially on small separations poorly represents the true covariance of the cosmic shear 2-point functions.

Hilbert et al. (2011) propose a different model for the convergence PDF, namely that of a *zero-mean shifted log-normal distribution*. In this approach the convergence at a given point on the sky is assumed to be of the form

$$\kappa(\boldsymbol{\theta}) = \exp[n(\boldsymbol{\theta})] - \kappa_0 \quad (15)$$

where  $n(\boldsymbol{\theta})$  is a Gaussian random field (not necessarily with a vanishing mean) and the *minimal convergence parameter*  $\kappa_0$  is chosen such that  $\langle \kappa \rangle = 0$ . Hilbert et al. (2011) show that from the corresponding PDF a model for the shear-shear contribution to the covariance matrix can be derived. Considering only the most important terms they also provide a simplified log-normal covariance, which reads

$$\begin{aligned}C_{\pm,\pm}^{ss}(\theta_1, \theta_2) &= \frac{1}{\pi A} \int d\ell \ell J_{0/4}(\ell\theta_1) J_{0/4}(\ell\theta_2) P_{\kappa}^2(\ell) \\ &\quad + \frac{8\pi}{\kappa_0^2 A} \xi_{\pm}(\theta_1) \xi_{\pm}(\theta_2) \int_0^{\theta_A} d\theta \theta \xi_{\kappa}(\theta),\end{aligned}\quad (16)$$

where  $\theta_A$  represents the 'radius' of the survey, given by

$$\theta_A = \sqrt{\frac{A}{\pi}}. \quad (17)$$

Comparing equation 16 to equation 14 one can see that the simplified log-normal approximation to  $C_{\pm,\pm}^{ss}$  consists of only one correction term to the Gaussian model. In our paper, we

will simulate log-normally distributed convergence fields and use equation 16 to compute the cosmic variance part of our model covariance.

### 2.2.3 Finite bin width

The expressions presented above for the covariance of  $\hat{\xi}_{\pm}$  are derived under the assumption of small angular bins (Schneider et al. 2002). However, in order to reduce the number of data points, in a likelihood analysis one will usually choose thick angular bins (see e.g. Kilbinger et al. (2013), Becker et al. in Preparation). Hence, in section 5.2 we will also investigate situations where the relative bin width is  $\sim 0.3$ , i.e. where the assumption of small bins does not hold.

In order to still get a good model for the covariance of our simulations we proceed as follows: We compute the log-normal model for the covariance, eqn. 16, for a set of very small angular bins  $\tilde{\theta}_i, i = 1, \dots, \tilde{N}$ . Then we apply a linear transformation that takes the large data vector of the small angular bins to a smaller data vector by putting together  $p$  neighbouring bins of the old data vector,

$$\begin{aligned} \theta_i &= \sum_{j=p \cdot i}^{p \cdot (i+1) - 1} \tilde{\theta}_j N_p(\tilde{\theta}_j) / \sum_{j=p \cdot i}^{p \cdot (i+1) - 1} N_p(\tilde{\theta}_j) \\ \hat{\xi}(\theta_i) &= \sum_{j=p \cdot i}^{p \cdot (i+1) - 1} \hat{\xi}(\tilde{\theta}_j) N_p(\tilde{\theta}_j) / \sum_{j=p \cdot i}^{p \cdot (i+1) - 1} N_p(\tilde{\theta}_j), \end{aligned} \quad (18)$$

where  $N_p(\tilde{\theta}_j)$  is the number of pairs in the  $j$ th bin of the finer data vector.

The same linear transformation is then applied to the covariance matrix of the large data vector to get the covariance matrix of the compressed data vector. We find that for  $\hat{\xi}_+$  this makes almost no difference. However, for  $\hat{\xi}_-$  it decreases the mixed- and cosmic variance part of the covariance by  $\gtrsim 30\%$ . (The  $C_{\pm\pm}^{nn}$  term of the covariance is correct for any bin width).

## 3 LOG-NORMAL SIMULATIONS

It was shown by Hilbert et al. (2011), using the Millennium simulation, that the log-normal model gives a much more realistic description of the covariance of the cosmic shear 2-pt. functions than the Gaussian model. Hence in our paper we are simulating cosmic shear fields, for which the underlying convergence field has a log-normal PDF, in order to present a realistic test of internal covariance estimators.

Simon et al. (2004) described a quick method to simulate cosmic shear surveys based on a Gaussian convergence field for any given convergence-power-spectrum. On a quadratic grid in 2D-Fourier space they generate at each point  $\ell$  of the grid a value of the convergence

$$\hat{\kappa}(\ell) = \kappa_1(\ell) + i\kappa_2(\ell)$$

where the components  $\kappa_i(\ell)$  are drawn from a Gaussian distribution with zero mean and variance

$$\sigma_{\ell}^2 = \frac{1}{2V} P_{\kappa}(\ell).$$

Here  $P_{\kappa}$  is the desired convergence power-spectrum and  $V$  is given in terms of the grid spacing<sup>3</sup>  $\Delta\ell$  as

$$V = \left( \frac{2\pi}{\Delta\ell} \right)^2.$$

In order to achieve a convergence field that is real valued in angular space one has to impose the condition

$$\hat{\kappa}(\ell) = \hat{\kappa}^*(-\ell)$$

and in Fourier space the shear field is related to the convergence field by the equation<sup>4</sup>

$$\hat{\gamma}(\ell) = \frac{\ell_1^2 - \ell_2^2 + 2i\ell_1\ell_2}{\ell^2} \hat{\kappa}(\ell). \quad (19)$$

A Fourier transform then gives the shear field in angular space.

To generate a log-normally distributed convergence field we have to recall that in the shifted log-normal approximation  $\kappa(\theta)$  is of the form

$$\kappa(\theta) = \exp[n(\theta)] - \kappa_0 \quad (20)$$

where  $n(\theta)$  is a Gaussian random field with mean  $\mu$  and variance  $\sigma^2$  and  $\kappa_0$  is chosen such that  $\langle \kappa \rangle = 0$ . The main idea in generating such a random field is to generate the Gaussian field  $n(\theta)$  with the method of Simon et al. (2004) and transform it into  $\kappa(\theta)$  via equation 20.

According to Martin et al. (2012); Takahashi et al. (2014) the power spectrum of  $n$ ,  $P_n$ , can be computed from  $P_{\kappa}$  as follows: First the 2-pt. function of  $\kappa$  is related to the 2-pt. function of  $n$  via (see e.g. equation B.8 of Hilbert et al. 2011):

$$\xi_{\kappa}(\theta) = \kappa_0^2 \cdot (\exp[\xi_n(\theta)] - 1). \quad (21)$$

Using also equation 3 (and its inverse) one can compute  $P_n$  from  $P_{\kappa}$  in the following steps:

$$\begin{aligned} \xi_{\kappa}(\theta) &= \frac{1}{2\pi} \int_0^{\infty} d\ell \ell P_{\kappa}(\ell) J_0(\ell\theta) \\ \rightarrow \xi_n(\theta) &= \ln(\xi_{\kappa}(\theta)/\kappa_0^2 + 1) \\ \rightarrow P_n(\ell) &= 2\pi \int_0^{\infty} d\theta \theta \xi_n(\theta) J_0(\ell\theta). \end{aligned} \quad (22)$$

This way  $n$  will have a mean value of zero and the appropriate mean value,

$$\mu = \kappa_0 - \frac{\sigma^2}{2}, \quad (23)$$

has to be added in order to have  $\langle \kappa \rangle = 0$ . With equation 19 one can then compute the Fourier modes of the shear field.

We use the simulations described above to generate shear fields. Our power spectrum is computed using the NICA EA code<sup>5</sup> and it follows the cosmology of the Millennium simulation that was also used by Hilbert et al. (2011). In harmonic space our grid has a spacing of  $\Delta\ell = 2$  and a total number of  $(2^{16})^2$  grid points. Out of the Fourier transformed grid in angular space we cut a region of  $(70 \text{ deg})^2$ , onto which we place galaxies with a density of  $20 \text{ arcmin}^{-2}$  (we will use

<sup>3</sup>  $V$  is the volume of the grid in angular space.

<sup>4</sup> see equation 25 of Simon et al. (2004) or equation 8 of Joachimi et al. (2008)

<sup>5</sup> by Kilbinger et al., [www.cosmostat.org/software/nicaea/](http://www.cosmostat.org/software/nicaea/)

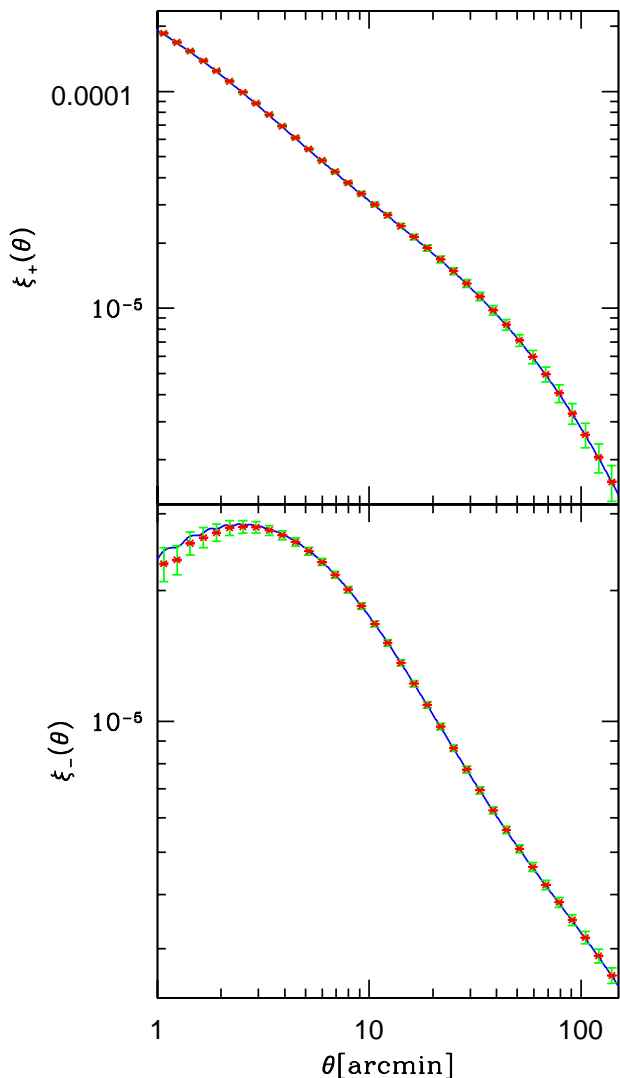


**Figure 1.** Comparison of the mean correlation functions from 1000 simulations (red dots) and the input model (blue line). The red error bars show the standard deviation of the mean and the green errorbars show the standard deviation of the single correlation function measurements. We used the redshift distribution of Hilbert et al. (2011) to compute the input power spectrum and we also used their value of  $\kappa_0$  to generate the log-normal convergence. Note that in section 5.2 we will use a different configuration.

different densities in section 5.2). The shear grid is interpolated to the position of each galaxy and a Gaussian random shape noise of ellipticity dispersion  $\sigma_\epsilon = 0.3$  is added to get the total shape of the galaxy. Note that we simply added the shear signal and intrinsic ellipticity, hereby ignoring the effects of *reduced shear*.

We simulate the mock survey 1000 times to test its statistical properties against the expectation from our log-normal input model. In order to speed up the computations we decrease the number of galaxies with respect to our jackknife analysis by a factor of 5 while also decreasing the ellipticity dispersion by a factor of  $\sqrt{5}$ . This way the covariance expressions in equation 16 stay unaffected.

In figure 1 we show the mean measured correlation functions in the simulation. The correlation function measurement was carried out using the TREECORR tree code<sup>6</sup> using 35 logarithmic bins from  $\theta_{\min} = 1'$  to  $\theta_{\max} = 150'$ . The measured correlation functions and those derived from the input model agree well. However, at small angular scales the measured value of  $\xi_-$  differs significantly from the input modes. The reason is the artificial cut-off at high  $\ell$ -values in our Fourier grid which both in the model and the simulation introduces artefacts - as can be seen from the oscillatory behaviour of  $\xi_-$ . If the grid spacing  $\Delta\ell$  was increased this would instead introduce artefacts at high angular scales, as was also reported by Simon et al. (2004). Hence we stay with the set-up described above but for our jackknife analyses in section 5 we will only consider those bins in  $\xi_-$  that have  $\theta \gtrsim 4.5'$ . For  $\xi_+$  we continue to use a range of  $1' < \theta < 150'$ .

Figure 2 compares the sample covariance of the 1000 simulations to the predictions from equation 16. For  $\xi_+$  there seems to be a significant deviation between the measured variance and the log-normal model. However, the sample variance values at different angular scales are highly correlated. When transforming the covariance matrices into the eigenbasis of the model covariance (right-hand panel of figure 2), the variance values become uncorrelated and the systematic deviations disappear. Only for the smallest eigenvalues of the model covariance matrix (i.e. for large  $i$ ) a systematic deviation remains. This is probably due to imperfections in our simulations or in our expressions for the log-normal model itself.

#### 4 INTERNAL COVARIANCE ESTIMATION FOR TWO-POINT CORRELATION FUNCTIONS

Suppose the correlation functions  $\xi_\pm$  have been measured in finite bins around a set of angular distances  $\theta_i$ ,  $i = 1, \dots, d$ . Let  $\hat{\xi}$  be either one of the data vectors  $[\xi_\pm(\theta_1), \dots, \xi_\pm(\theta_d)]$  or the joint data vector of both correlation functions.

If  $\xi[\boldsymbol{\pi}]$  is a model for the measurement  $\hat{\xi}$  which depends on a set of parameters  $\boldsymbol{\pi}$ , then a common statistic for constraining the possible values of  $\boldsymbol{\pi}$  is the  $\chi^2$  statistic (Kilbinger & Schneider 2004), i.e.

$$\chi^2[\boldsymbol{\pi}] = (\hat{\xi} - \xi[\boldsymbol{\pi}])^T C^{-1} (\hat{\xi} - \xi[\boldsymbol{\pi}]), \quad (24)$$

where  $C$  is the covariance matrix of  $\hat{\xi}$ . One way to get the covariance matrix is to model it theoretically. As we have seen in section 2.2 the modelling of the covariance depends crucially on the PDF of the convergence field (Schneider et al. 2002; Hilbert et al. 2011; Sato et al. 2011) and neither the Gaussian nor the log-normal approximation match a realistic convergence PDF. Also, the model covariance matrix will depend on cosmological parameters itself which has, at least for small surveys, has to be taken into account when deriving parameter constraints (Eifler et al. 2009).

A way to get around modelling the covariance matrix directly is to use the sample covariance of measurements of the correlation functions in a set of independent N-body simulations (Taylor et al. 2013) which however still depends

<sup>6</sup> by Jarvis et al., [github.com/rmjjarvis/TreeCorr](https://github.com/rmjjarvis/TreeCorr)

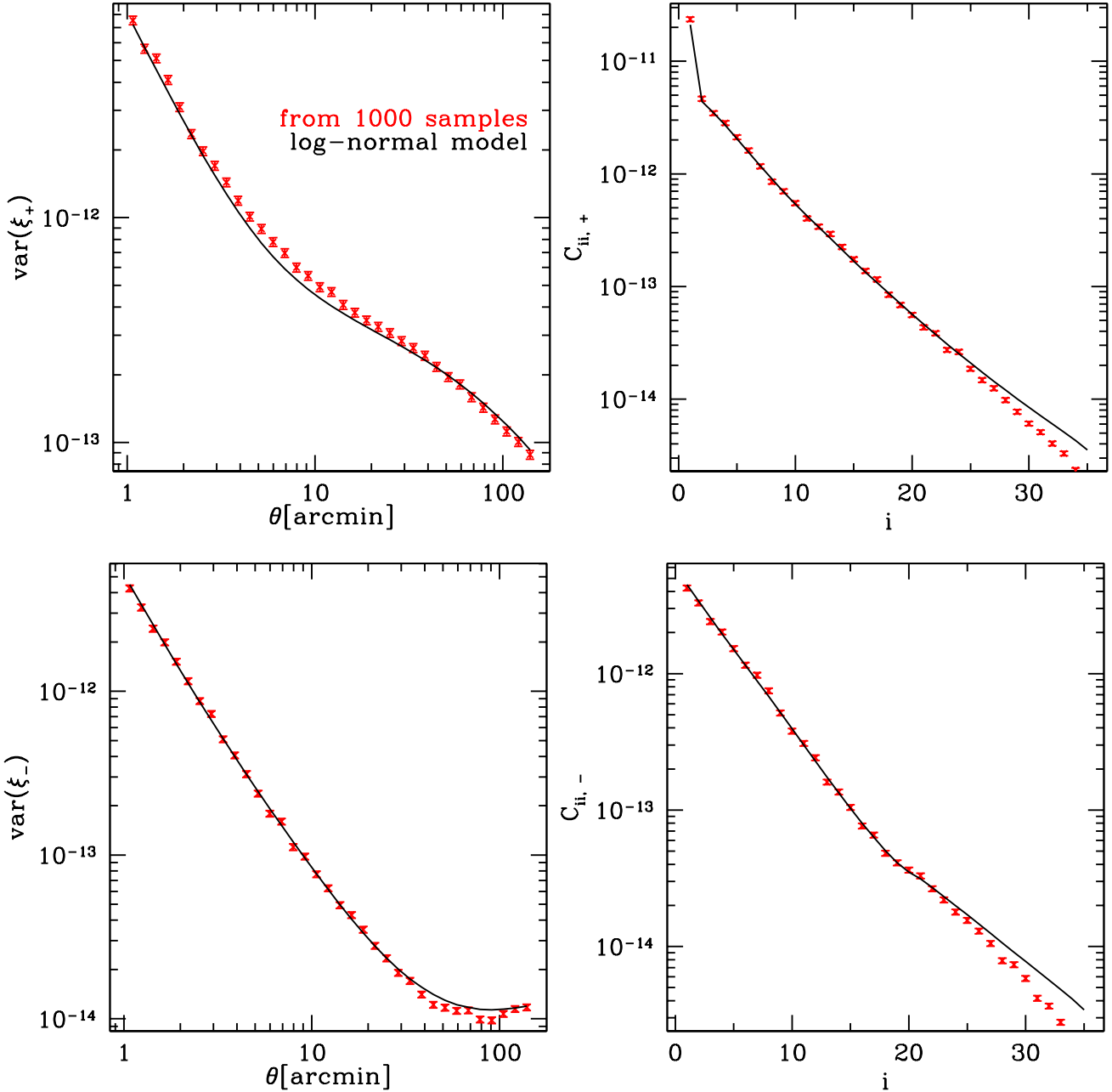


**Figure 2.** Left: sample variance from 1000 independent simulations compared to the log-normal input model. The errorbars are assuming a Wishart distribution, note however that the different sample variance values are correlated. Right: in the diagonal basis of the model covariance matrix the sample variance values should independently follow a  $\chi^2$ -distribution. The model and the simulations are consistent for the  $\approx 20$  largest eigenvalues of the model covariance matrix.

on the model parameters, i.e. on the assumption of a particular cosmological model. Another alternative to modelling the covariance matrix is to estimate it from the data itself. In the following we will introduce three different internal covariance estimation methods - the *sub-sample covariance*, the *delete-one-jackknife* and the *bootstrap* (cf. Norberg et al. 2009; Loh 2008).

#### 4.1 Subsample Covariance

Let us split the area  $A$  of our cosmic shear survey into  $N$  equally shaped and sized subregions of the area  $A_S = A/N$ . In each subregion  $\alpha = 1, \dots, N$ , a measurement of the data vector  $\hat{\xi}^\alpha$  can be carried out. Assuming that each sub-region has approximately the same number of galaxies and that the correlation functions are measured on scales much smaller than  $\sqrt{A_S}$  the measurement of  $\hat{\xi}$  in the whole survey is given

by

$$\hat{\xi} \approx \bar{\xi} := \frac{1}{N} \sum_{\alpha=1}^N \hat{\xi}^{\alpha}, \quad (25)$$

i.e. it is the mean values of the measurements in the sub-regions. If the measurements  $\hat{\xi}^{\alpha}$  are independent, then the  $ij$ -th element of their covariance matrix could be estimated by

$$\langle \Delta \hat{\xi}_i^{\alpha} \Delta \hat{\xi}_j^{\alpha} \rangle \approx \frac{1}{N-1} \sum_{\beta=1}^N (\hat{\xi}^{\beta} - \bar{\xi})_i (\hat{\xi}^{\beta} - \bar{\xi})_j, \quad (26)$$

where  $\Delta \hat{\xi}^{\alpha}$  is the difference between  $\hat{\xi}^{\alpha}$  and its expectation value

$$\xi = \langle \hat{\xi}^{\alpha} \rangle = \langle \hat{\xi} \rangle. \quad (27)$$

Accordingly, if the assumption of independent sub-regions were true, the covariance of the total measurement  $\hat{\xi}$  could be estimated by

$$\hat{C}_{\text{SSC}} = \frac{1}{N(N-1)} \sum_{\alpha=1}^N (\xi^{\alpha} - \bar{\xi}) (\xi^{\alpha} - \bar{\xi})^T. \quad (28)$$

We will call the estimator in equation 28 the *sub-sample covariance* (Norberg et al. 2009).

## 4.2 Jackknife

Another method of covariance estimation that Norberg et al. (2009) investigate is the delete-one-jackknife. Instead of estimating the covariance of the measurements  $\xi^{\alpha}$  and rescaling it to the size of the whole survey the jackknife is considering the measurements

$$\hat{\xi}_{\pm}^{*\alpha}(\theta) = \frac{\sum_{\{i,j \text{ not in } \alpha\}} (\epsilon_t^i \epsilon_t^j \pm \epsilon_x^i \epsilon_x^j) \cdot \Delta_{\theta}(|\theta_i - \theta_j|)}{\sum_{\{i,j \text{ not in } \alpha\}} \Delta_{\theta}(|\theta_i - \theta_j|)}, \quad (29)$$

i.e. the *jackknife-sample*  $\alpha$  is generated by cutting out the subregion  $\alpha$  and measuring the correlation functions in the rest of the survey - see also figure 5. The jackknife estimate for the covariance matrix is then given by (Efron 1982; Norberg et al. 2009)

$$\hat{C}_{\text{jack}} = \frac{N-1}{N} \sum_{\alpha=1}^N (\xi^{*\alpha} - \bar{\xi}^*)^T (\xi^{*\alpha} - \bar{\xi}^*), \quad (30)$$

where  $\bar{\xi}^*$  is the mean of all jackknife measurements.

If we again assume that all subregions have the same galaxy density and that the correlation functions are measured on scales much smaller than the sub-region size then  $\xi^{*\alpha}$  is approximately given by

$$\xi^{*\alpha} \approx \frac{1}{N-1} \sum_{\beta \neq \alpha} \hat{\xi}^{\beta}. \quad (31)$$

From this it also follows that

$$\begin{aligned} \xi^{*\alpha} - \bar{\xi}^* &\approx \frac{N \cdot \bar{\xi} - \hat{\xi}^{\alpha}}{N-1} - \frac{1}{N} \sum_{\beta} \xi^{*\beta} \\ &= \frac{N \cdot \bar{\xi} - \hat{\xi}^{\alpha}}{N-1} - \frac{1}{(N-1) \cdot N} \sum_{\beta} \sum_{\gamma \neq \beta} \hat{\xi}^{\gamma} \\ &= \frac{1}{N-1} \sum_{\beta \neq \alpha} \hat{\xi}^{\beta} - \frac{N-1}{(N-1) \cdot N} \hat{\xi}^{\alpha} \\ &= \frac{N \cdot \bar{\xi} - \hat{\xi}^{\alpha}}{N-1} - \bar{\xi} \\ &= \frac{\bar{\xi} - \hat{\xi}^{\alpha}}{N-1}. \end{aligned} \quad (32)$$

Inserting this into the definition of  $\hat{C}_{\text{jack}}$  gives exactly the subsample covariance  $\hat{C}_{\text{SSC}}$ , i.e. on small angular scales the two methods are approximately equivalent<sup>7</sup>.

## 4.3 Bootstrap Covariance

The so called *block bootstrap* estimator of the covariance also divides the data into sub-samples. If the data is split into  $N$  sub-regions, then a number of  $N_{\text{boot}}$  bootstrap re-samplings of the data are generated by randomly drawing with replacement  $N$  of the sub-samples and combining them into one re-sampled data set (Norberg et al. 2009; Nordman & Lahiri 2007; Loh 2008; Efron 1982). If the correlation function measured in the re-sampled data  $i$  ( $i = 1, \dots, N_{\text{boot}}$ ) is called  $\xi^{\text{boot},i}$ , then the bootstrap estimate of the covariance is given by

$$\hat{C}_{\text{boot}} = \frac{1}{N_{\text{boot}} - 1} \sum_{i=1}^{N_{\text{boot}}} (\xi^{\text{boot},i} - \bar{\xi}^{\text{boot}})^T (\xi^{\text{boot},i} - \bar{\xi}^{\text{boot}}), \quad (33)$$

where  $\bar{\xi}^{\text{boot}}$  is now the mean of all  $\xi^{\text{boot},i}$ .

The question arises, whether one should consider the single galaxies or the galaxy pairs as the actual data (cf. section 4.5). In what we will call *galaxy-bootstrap* one simply adds a copy of all galaxies in a sub-region  $\alpha$  to the re-sampled data set  $i$  each time the sub-region  $\alpha$  gets drawn.

In the *pair-bootstrap* one adds all pairs in sub-region  $\alpha$  to the list of pairs that is used to compute  $\xi^{\text{boot},i}$ . The difference between the two bootstrap schemes is mainly the following: if the sub-region  $\alpha$  gets drawn  $n$  times, then each pair in  $\alpha$  gets a weight of  $n$  in the pair-scheme and a weight  $n^2$  in the galaxy-scheme.

Note that the pair-bootstrap is very similar to what Loh (2008) describes as *marked point bootstrap*, the only difference being, that we chose to split pairs between sub-regions evenly among these regions (a more detailed explanation is given in section 4.5).

We will see in section 5 that the galaxy-bootstrap severely overestimates the covariance. The other covariance estimators perform very similar to each other and suffer from similar systematics. We will explain them in the following. Since it will be shown in section 5, that all internal covariance estimators perform very similar, we will focus the rest of this section on the jackknife method.

<sup>7</sup> This is no general statement on the jackknife method. It holds only in our particular situation.

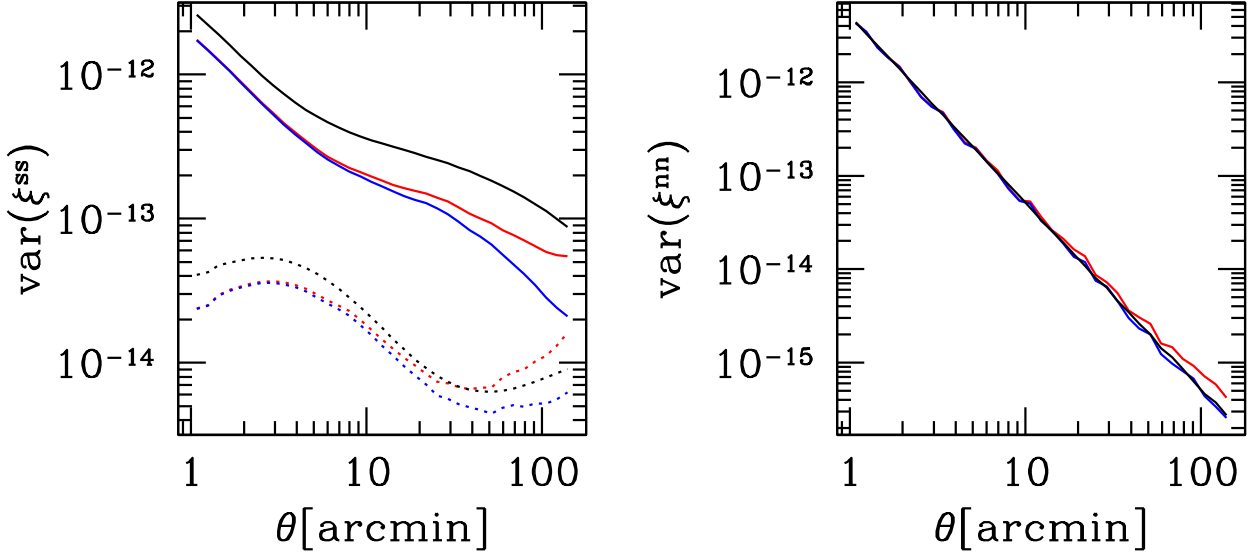


**Figure 3.** Left: Different variance estimates for  $\hat{\xi}_+$  (solid lines) and  $\hat{\xi}_-$  (dotted lines) in a mock catalog without shape noise. The red lines show the galaxy-jackknife estimate (c.f. section 4.5), the blue lines show the pair-jackknife estimate and the black lines show the log-normal input model. Right: Jackknife estimates of the variance of  $\hat{\xi}_+$  in a mock catalog that only consists of shape noise. It is only in this situation (and in the pair-jackknife scheme) that jackknife estimation of the covariance yields unbiased results.

#### 4.4 Correlation of sub-samples

The jackknife method (and also the *sub-sample covariance* and the *bootstrap covariance*) relies on the assumption that the sub-samples into which the data are split are independent, i.e. that there is no correlation of the measurements of the correlation functions in the different sub-samples,

$$\langle \Delta \hat{\xi}_i^\alpha \Delta \hat{\xi}_j^\beta \rangle \stackrel{!}{=} 0, \text{ for } \alpha \neq \beta. \quad (34)$$

If they are instead correlated, the true covariance matrix will be underestimated by internal estimators (Nordman & Lahiri 2007).

In a sense, if the sub-regions are correlated the measurements  $\hat{\xi}^\alpha$  ‘don’t vary enough’ to yield the true covariance of  $\hat{\xi}$ . However, the more adequate way to think about this is as follows: Both jackknife and sub-sample covariance (and bootstrap) assume that the covariance matrix of  $\hat{\xi}$  is inversely proportional to the survey area  $A$ . Hence they estimate the covariance of sub-regions of the size  $A_S$  within the data and then rescale it to the total area,

$$C = \frac{A_S}{A} \cdot C_S = \frac{1}{N} \cdot C_S, \quad (35)$$

where  $N$  is again the number of sub-regions. But already from the log-normal model for the cosmic variance part of the covariance it can be seen, that this rescaling is not valid:

$$\begin{aligned} C_{\pm\pm}^{ss}(\theta_1, \theta_2) &= \frac{1}{\pi A} \int d\ell \ell J_{0/4}(\ell\theta_1) J_{0/4}(\ell\theta_2) P_\kappa^2(\ell) \\ &+ \frac{8\pi}{\kappa_0^2 A} \xi_\pm(\theta_1)\xi_\pm(\theta_2) \int_0^{\theta_A} d\theta \theta \xi_\kappa(\theta). \end{aligned} \quad (36)$$

The second term in this equation may be proportional to  $1/A$ , but the upper integral boundary also depends on the

survey diameter  $\theta_A$ . As  $A$  increases, the covariance therefore decreases slower than  $1/A$ . Hence assuming  $1/A$  scaling when extrapolating from the covariance in the smaller sub-fields to the covariance in the larger full area, as is typically done in internal covariance estimation, underestimates the full covariance. Note, that this is equivalent to saying that close sub-regions are correlated and that this is also the reason for the *finite area* effect that was discussed before.

In figure 3 we demonstrate this effect. The left-hand panel shows jackknife estimates of the variance of  $\hat{\xi}_\pm$  in a simulated survey where the shape noise was put to zero. Both the variance of  $\hat{\xi}_+$  and  $\hat{\xi}_-$  are severely underestimated by the delete-one-jackknife and the situation is very similar for the sub-sample and the pair-bootstrap covariance (which are not shown here, see figure 6 for a comparison). An exception are large angular scales, at which at least for  $\hat{\xi}_-$  an overestimation of the variance happens. Here, another effect comes into play which will be discussed in the next subsection.

On the other hand, the shape noise in the sub-regions is completely uncorrelated. Hence the shape noise component of the covariance can be internally estimated without bias as can be seen from the right-hand panel of figure 3 where a pure shape noise catalog was generated.

The fact that sub-samples should be as uncorrelated as possible is also the reason why the jackknife re-sampling of the data should be done in coherent patches. If instead the data would be randomly divided into sub-samples then the shear correlations in the sub-samples would be almost identical. Hence, only the shape-noise contributions to the covariance would be measured by such an estimator.



#### 4.5 Galaxy pairs crossing between sub-samples

A problem specific to the internal covariance estimation for two-point correlation functions is the question of what to do with pairs of galaxies where each galaxy lies in a different sub-region of the data.

In fact the pieces of information in a cosmic shear survey are not the individual galaxy shapes but the pairs of galaxy shapes. But each such pair of shapes will be left out *twice* (instead of once) if the jackknife re-sampling is done with respect to the individual galaxies (cf. figure 5). This increases the variance between the jackknife samples and hence the covariance estimate.

The situation becomes more clear for the sub-sample covariance: Here, the pairs crossing between sub-regions are completely ignored. Hence, one is re-sampling a data set that has *less* information than the total measurement of  $\xi_{\pm}$  and a larger variance. Note, that this does not only influence the shape-noise part of the covariance but - as can be seen from the left-hand panel of figure 3 - also the cosmic variance part. The reason is that galaxies at the edge of a sub-region contribute less terms to the correlation function measurement than galaxies in the center of the sub-region (c.f. figure 4), i.e. the area of the sub-patch is not uniformly probed by the galaxy pairs and the measured shear correlations are dominated by the inner parts of the patch. In contrast to the correlation of sub-samples discussed before, this increases the cosmic variance between the sub-samples and can bias the covariance estimate high on large angular scales.

This effect can in principle be resolved by re-sampling the set of pairs (instead of the set of galaxy shapes), i.e. by defining the sub-measurement  $\hat{\xi}_{\pm}^{\alpha}$  as

$$\hat{\xi}_{\pm}^{\alpha}(\theta) = \frac{\sum_{\text{pairs in } \alpha} (\epsilon_t^i \epsilon_t^j \pm \epsilon_x^i \epsilon_x^j) + \sum_{\text{half of cross pairs}} (\epsilon_t^i \epsilon_t^j \pm \epsilon_x^i \epsilon_x^j)}{N_{\text{pairs}}} . \quad (37)$$

How this resampling of galaxy pairs can be done is illustrated in figure 5. Especially one has to make sure that each galaxy pair enters exactly one of the  $\hat{\xi}^{\alpha}$ <sup>8</sup>. We call this procedure the *pair-jackknife* while we will call the standard jackknife procedure *galaxy-jackknife*. The pair-jackknife is preferable in surveys whose covariance is shape noise dominated. On the right-hand panel of figure 3 you can see that it estimates the shape noise part of the covariance very accurately, while the galaxy-jackknife overestimates this contribution. A downside of the pair-jackknife is that the shear signals in the sub-measurements  $\hat{\xi}^{\alpha}$  become even more correlated, as can also be seen from the left-hand panel of figure 3.

It should be mentioned that both jackknife schemes can be most easily implemented in the *marked point* formalism for re-sampling that was given by Loh (2008).

#### 4.6 Stability and Inversion of the Covariance Estimate

All effects that bias the internal covariance estimate can in principle be minimized by dividing the data into very large sub-regions. This decreases both the correlation of the different sub-regions and the influence of pairs crossing between sub-regions. However, this also decreases the possible number of re-samplings and hence increases the variance of the covariance estimator itself!

In order to derive constraints on the number of re-samplings let us assume that we are in the limit where the correlations between sub-regions are small. Small here means that

$$\langle \Delta \hat{\xi}_i^{\alpha} \Delta \hat{\xi}_j^{\beta} \rangle \ll \langle \Delta \hat{\xi}_i^{\alpha} \Delta \hat{\xi}_j^{\alpha} \rangle , \text{ for } \alpha \neq \beta . \quad (38)$$

As explained before, this is the only limit in which internal covariance estimation is valid! In this limit the pair-jackknife is exactly equivalent to the pair-version of the sub-sample covariance, i.e. to equation 28 when  $\hat{\xi}^{\alpha}$  is computed with equation 37. Furthermore, in this limit the sub-sample covariance is just a rescaled version of the sample covariance of the sub-regions. Hence - in the limit considered here and under the assumption that the underlying field is Gaussian - the internal covariance estimates are distributed according to a Wishart distribution (cf. Taylor et al. 2013).

The most important consequence of this is that the inverse of the covariance matrix estimate will be a biased estimate of the true inverse covariance matrix, and the bias is approximately given by (Hartlap et al. 2007; Taylor et al. 2013):

$$\langle \hat{C}_{\text{SSC}}^{-1} \rangle \approx \frac{N-1}{N-d-2} C_{\text{true}}^{-1} , \quad (39)$$

where  $N$  is the number of sub-regions and  $d$  is the number of data points in  $\hat{\xi}$ . Especially, this factor has to be accounted for when computing the  $\chi^2$  statistic, eq. 24, i.e. it has an influence on the constraints derived on cosmological parameters when using internal covariance estimation.

Taylor et al. (2013) also give constraints on  $N$  with respect to  $d$  when a certain accuracy in the final parameter constraints is demanded. However, their results were derived for covariance estimates with an exact Wishart distribution. Furthermore, they are ignoring the impact that the variance in the inverted covariance estimate has on parameter constraints, which is investigated by Taylor & Joachimi (2014). Nevertheless we take the criterion of Taylor et al. (2013),

$$N \stackrel{!}{>} \frac{2}{\epsilon^2} + (d+4) , \quad (40)$$

where  $\epsilon$  is the required fractional accuracy on parameter constraints, as a guideline also for internal covariance estimation.

<sup>8</sup> respectively: each galaxy pair is left out in exactly one of the jackknife re-samplings  $\hat{\xi}^{*\alpha}$

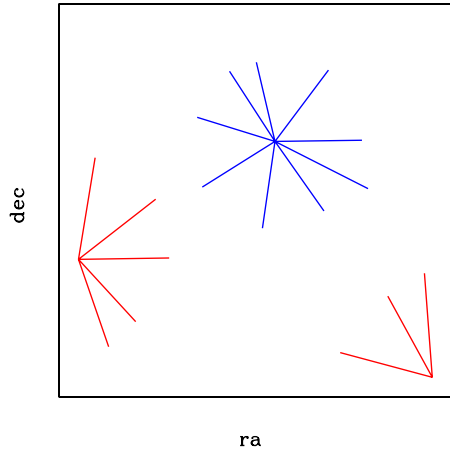


**Figure 4.** Galaxies at the edge of a sub-region (in red) contribute less pairs to the measurement of the correlation functions (i.e. to equation 5 applied to the sub-sample) than galaxies in the center of the sub-region (in blue). Consequently, the area of the sub-patch is not uniformly probed by the galaxy pairs. This increases the cosmic variance between sub-regions and biases the covariance estimates high. Hence, it has an opposite effect than the correlation of sub-samples, which biases the covariance estimates low. As you can see from the left-hand panel of figure 3, at large angular scales this can (in the galaxy-scheme, c.f. also figure 5) even lead to an overestimation of the cosmic variance of  $\xi_-$ .

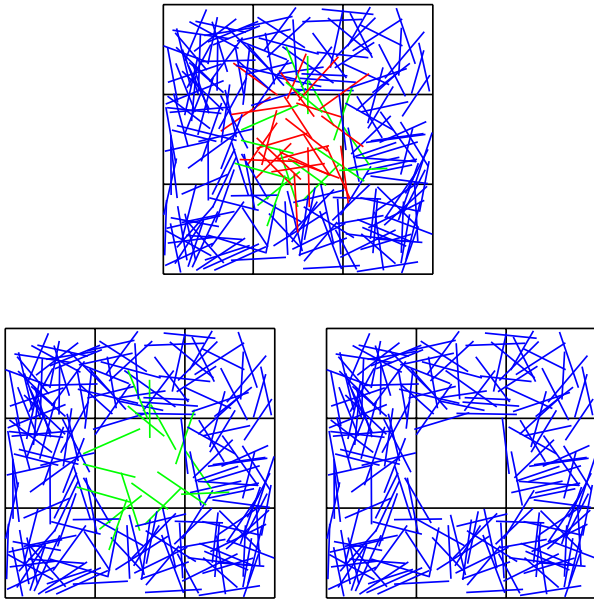


**Figure 5.** Two basic jackknife schemes for a set of galaxy pairs given by the top panel. In the galaxy-jackknife scheme (lower right)  $\xi^{*\alpha}$  is computed by cutting out all galaxy pairs that have at least one galaxy in the sub-region  $\alpha$ . In the pair-jackknife scheme (lower left) half of the pairs that cross from  $\alpha$  to another region (drawn in green) are taken into account for computing  $\xi^{*\alpha}$ , while only the other half (red) is discarded.

## 5 TESTING INTERNAL COVARIANCE ESTIMATORS ON SIMULATED COSMIC SHEAR SURVEYS

We will now use the simulations described in section 3 to test the performance of internal covariance estimators. The cosmology will be kept fixed to that of Hilbert et al. (2011), i.e. a flat  $\Lambda$ CDM universe with  $(\Omega_m, \Omega_b, \sigma_8, h_{100}, n_s) = (0.25, 0.045, 0.9, 0.73, 1.0)$ . First, we simulate a survey of  $(70 \text{ deg})^2$  and the redshift distribution of Hilbert et al. (2011),

$$p(z) = \frac{3z^2}{2z_0^3} e^{-\left(\frac{z}{z_0}\right)^{3/2}}, \quad \text{where } z_0 = \frac{1.0}{1.414}. \quad (41)$$

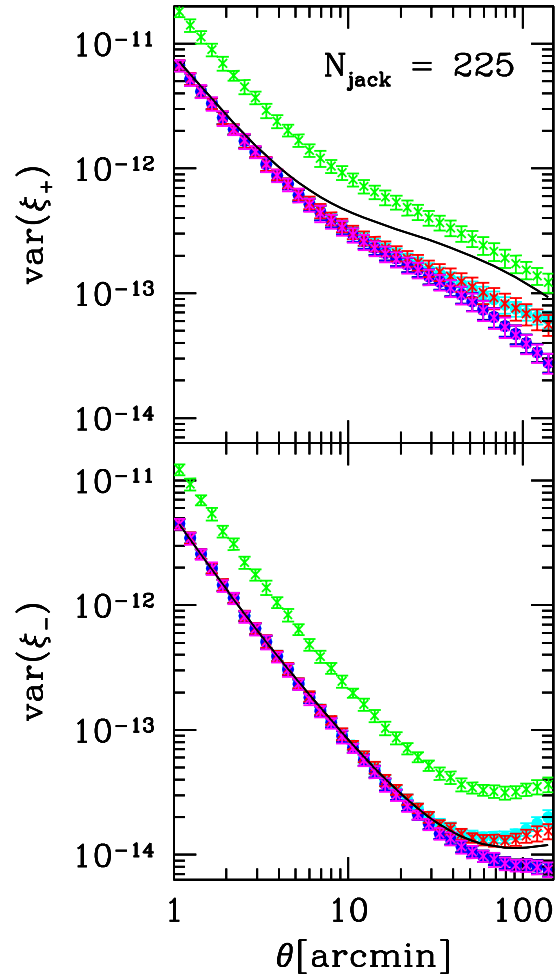


**Figure 6.** A comparison of the different internal estimation schemes when splitting the survey into  $N = 225$  sub-regions. Green: galaxy-bootstrap, purple: pair-bootstrap, red: galaxy-jackknife, blue: pair-jackknife and cyan: sub-sample covariance compared to the analytical covariance (black line). We show the sub-sample covariance only in the galaxy-scheme because in the pair-scheme it is almost identical to jackknife and bootstrap. As explained in section 4, at large angular scales the different treatment of galaxy pairs crossing between sub-region leads to an overestimation of the variance by the galaxy-scheme and an underestimation of the variance by the pair-scheme.

This distribution has a median redshift of 1.0. Hilbert et al. (2011) give a value of  $\kappa_0 = 0.032$  for this redshift distribution which we hence also employ to generate our log-normal fields. A total number of 352.8 Mio. galaxies is placed onto the survey corresponding to a source density of  $20 \text{ arcmin}^{-2}$ . Shape noise with an ellipticity dispersion per component of  $\sigma_\epsilon = 0.3$  is then added to each galaxy.

We carry out 50 independent realizations of this survey. In each survey we measure the correlation functions in the range and binning that was explained in section 3. We then estimate the covariance of the measured correlation functions using the different internal estimation schemes that were introduced in section 4. Throughout this section - except for subsection 5.2 - we consider the log-normal model that was explained in section 2.2 as the *true* covariance of the simulated surveys. This is justified by the fact that our results don't change if we instead use the sample covariance of 1000 independent realisations that was presented in section 3.

In figure 6 we compare the sub-sample, jackknife and bootstrap estimates of the diagonal elements of the covariance matrix (both in the galaxy- and pair-scheme) when splitting the survey into  $N = 225$  sub-regions. In the pair-scheme all three internal estimators perform almost identical. This is not surprising, because in that scheme the bootstrap is just an approximation to the sub-sample covariance and sub-sample and jackknife covariance are by definition very similar. In the galaxy-scheme the bootstrap severely overestimates to variance. This demonstrates that not the single galaxies but the pairs of galaxies have to be considered as the pieces of information in a cosmic shear survey, and hence bootstrap re-sampling has to be carried out with respect to the pairs. As explained in section 4.5, in the galaxy-jackknife scheme the two effects of correlated sub-regions and false re-sampling of pairs partly cancel each other. Hence the galaxy-jackknife comes closest to the true variance at large scales. The performance of the sub-sample covariance (in the galaxy-scheme) only slightly differs from that.

Because of its severe overestimation of the variance we will ignore the galaxy-bootstrap from now. Since the other estimators perform very similar within the pair- and jackknife-scheme, we will furthermore restrict the following analyses to the pair-jackknife and the galaxy-jackknife. We now investigate the influence of sub-region size on internal covariance estimation. Hence we split the surveys into 3 different numbers of sub-regions:  $10^2$ ,  $15^2$  and  $20^2$ .

In figure 7 we compare the mean value of the 50 jackknife estimates of the variance of  $\hat{\xi}_\pm$  (the diagonal elements of the covariance matrix) to the true underlying log-normal model. The errorbars represent the standard deviation of the 50 jackknife estimates, i.e. they illustrate the noise of the internal estimators. You can see in this figure the biases in the jackknife estimates that we explained in the previous section. For  $\xi_+$ , both jackknife schemes underestimate the variance. At large scales, this is in the galaxy-jackknife scheme partly compensated by the false re-sampling of galaxy pairs. For  $\xi_-$ , the pair-jackknife underestimates the variance while the galaxy-jackknife overestimates it.  $\xi_-$  is a much more local measure in the sense that the different sub regions are less correlated in  $\hat{\xi}_-$  and that the covariance matrix is much more dominated by the shape noise contributions. Hence,

the severe systematic underestimation of the variance that can be seen for  $\xi_+$  does not appear as strongly for  $\xi_-$ .

When increasing the number of sub-regions for the jackknife estimators, the noise in the variance estimates becomes smaller but the deviations from the true variance also become stronger. This is because for smaller sub-regions the estimated  $\hat{\xi}^\alpha$  become more correlated and because there will be more galaxy pairs crossing from one sub-region to another.

## 5.1 Constraints on cosmological Parameters

We will now take the 50 simulations as mock observations and try to constrain the dark matter density parameter  $\Omega_m$  and the power spectrum normalization  $\sigma_8$ . To do so we sample the  $\Omega_m$ - $\sigma_8$  plane on a fine grid while keeping the other cosmological parameters fixed. Following a Bayesian approach we take the probability density in the parameter space to be proportional to the likelihood,

$$p(\boldsymbol{\pi}) \sim \mathcal{L}(\boldsymbol{\pi}) \sim \exp\left(-\frac{1}{2}\chi^2[\boldsymbol{\pi}]\right), \quad (42)$$

where we assume our data vector  $\hat{\boldsymbol{\xi}}$  to be Gaussian such that

$$\chi^2[\boldsymbol{\pi}] = (\hat{\boldsymbol{\xi}} - \boldsymbol{\xi}[\boldsymbol{\pi}])^T C^{-1} (\hat{\boldsymbol{\xi}} - \boldsymbol{\xi}[\boldsymbol{\pi}]). \quad (43)$$

Here  $\boldsymbol{\xi}[\boldsymbol{\pi}]$  are our model predictions for  $(\hat{\boldsymbol{\xi}})$  which we again compute with the NICAFA package. We are assuming a prior of  $\Omega_m \in [0.1, 0.4]$  and  $\sigma_8 \in [0.8, 1.1]$ , which is well centered around our input cosmology. For  $C$  we will either insert the log-normal model covariance or the jackknife estimates of the covariance. We will de-bias the inverse of the latter in the way explained in section 4.6. Note that the reasoning in section 4.6 is in principle only valid for the pair-jackknife. And also for the pair-jackknife it is only valid in the case of almost uncorrelated sub-regions. We will nevertheless carry out the de-biasing in the same way for both jackknife schemes. Furthermore, we will also ignore the variance of the inverted covariance estimate (Taylor & Joachimi 2014), as explained in the end of section 4. Our data vector  $\hat{\boldsymbol{\xi}}$  will be either  $\hat{\xi}_+$  or  $\hat{\xi}_-$  or the joint data vector of both correlation functions, in which case we will also take into account the cross covariance between the two.

For each mock observation  $\hat{\boldsymbol{\xi}}$  and for each available covariance matrix we use equation 42 to compute marginalised  $1\sigma$  constraints on  $\Omega_m$  and  $\sigma_8$ , i.e. we consider the marginalised probability densities

$$\begin{aligned} p_\Omega(\Omega_m) &= \int d\sigma_8 p(\Omega_m, \sigma_8) \\ p_\sigma(\sigma_8) &= \int d\Omega_m p(\Omega_m, \sigma_8) \end{aligned} \quad (44)$$

and we define  $1\sigma$  confidence interval to be that interval around the best fit parameter value which encloses  $\sim 68\%$  of the probability and which has equal values of the probability density at each interval boundary<sup>9</sup>.

Because of the strong degeneracy between  $\Omega_m$  and  $\sigma_8$  (Kilbinger et al. 2013; Kilbinger & Schneider 2004), even

<sup>9</sup> Without the last statement the definition of the  $1\sigma$  confidence interval would be ambiguous.

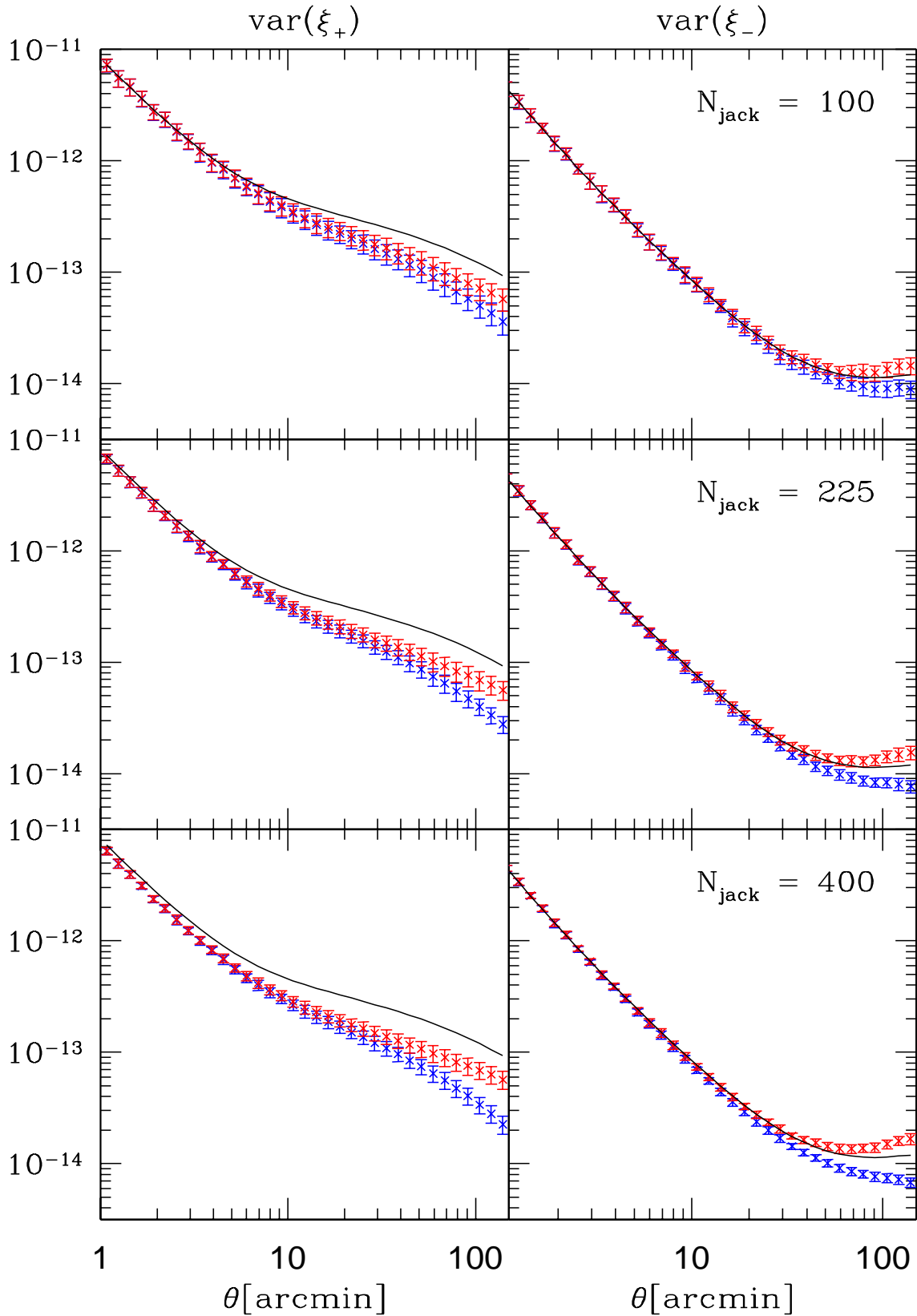


**Figure 7.** Mean values of 50 jackknife estimates of the variance of  $\xi_+$  (left) and  $\xi_-$  (right). Galaxy-jackknife was used for the red points while pair-jackknife was used for the blue points. The black line corresponds to the log-normal input model of the simulations.

little uncertainties in the modelling of  $\xi[\pi]$ <sup>10</sup> or in our simulations could shift the best-fit values of the parameters along the degeneracy. Fortunately, this does not affect our analysis because we only have to compare the constraints derived from the jackknife covariance estimates to the constraints obtained from the true (log-normal) covariance matrix. Furthermore, our results don't change noticeably, if instead of the log-normal covariance matrix we use the sample covariance estimated from 1000 simulations (c.f. section 3). Hence in any case, our analysis provides a fair test of internal covariance estimators.

In figure 8 we show the mean values of the upper and lower boundaries on  $\Omega_m$  and  $\sigma_8$  as well as their mean best fit value for different numbers of jackknife re-samplings (red points and errorbars). The mean is taken with respect to all 50 confidence intervals we computed from the 50 mock observations. We also compare the jackknife constraints to those we get when using the true covariance matrix (blue lines). These figures only show the results for the galaxy-jackknife, which in the situation considered here yields the best agreement with the true covariance.

We compare galaxy-jackknife and pair-jackknife in figure 9. Here we show the mean width of the confidence intervals obtained with galaxy-jackknife, pair-jackknife and the true covariance matrix. For  $\xi_-$ , the width of the confidence intervals agrees well with the confidence intervals obtained from the true covariance matrix. In fact, even for the pair-scheme and even for 400 jackknife re-samplings the width of the confidence intervals from  $\xi_-$  alone is not underestimated. This seems to contradict figure 7, where the pair-scheme systematically underestimates the covariance. One reason for this is probably, that the variance in the inverted covariance estimate increases parameter uncertainties (Taylor & Joachimi 2014). Note especially, that this is not the same effect as the de-biasing in eqn. 4.6. For  $\xi_+$ , the strong underestimation of the covariance matrix by jackknife also leads to an underestimation of the uncertainties on  $\Omega_m$  and  $\sigma_8$ . Again one can see that the variance in the width of the confidence intervals (the errorbars in figure 9) becomes smaller, when more jackknife re-samplings are used. In turn, this increases the overall underestimation of the uncertainties. If both correlation functions are combined and 225 re-samplings are used, the parameter uncertainties are underestimated by  $\sim 10\%$ .

We have not shown results from the pair-jackknife estimates in figure 8, but the best fit values of  $\Omega_m$  and  $\sigma_8$  agree very well between the two jackknife schemes (i.e. within the green errorbars in figure 8), if only  $\hat{\xi}_+$  or  $\hat{\xi}_-$  are used to constrain the parameters. In figure 10 we compare the pair-jackknife and galaxy-jackknife best fit values when using the *full* data vector. Here the pair-jackknife seems to yield a bias of the best fit values with respect to the true covariance.

The above results indicate that internal covariance estimation can reproduce the constraints on parameters from the true covariance quite well, especially when the galaxy-jackknife scheme is used. However, these results are not generalizable. In general, internal estimation of the covariance works best if the covariance matrix is shape noise dominated.

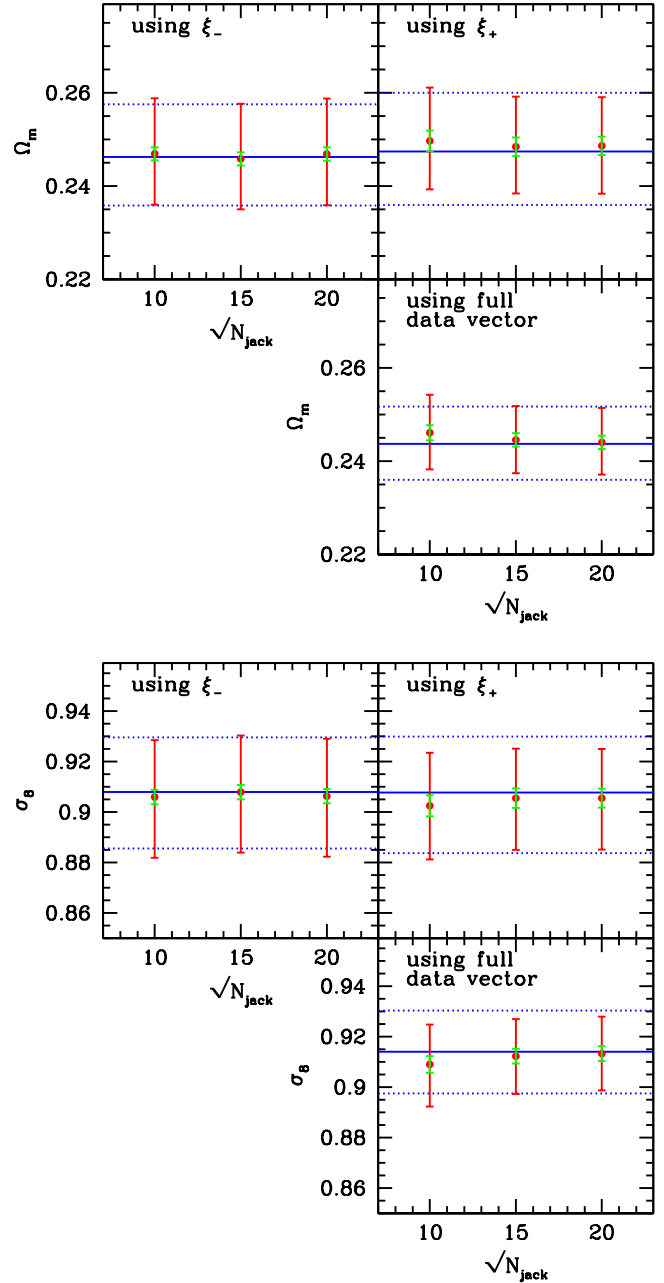


**Figure 8.** Mean  $1\sigma$  constraints on  $\Omega_m$  and  $\sigma_8$  using galaxy-jackknife (red errorbars). The green errorbars show the standard deviation of the mean best-fit values (i.e. the standard deviation of the best fit values divided by  $\sqrt{50}$ ). The blue lines indicate the constraints that are obtained when the true covariance is used in each mock catalog. Note that the error bars are very symmetric. For surveys as big as our simulations the constraining power becomes large enough to turn the - usually *banana* shaped - degeneracy between  $\Omega_m$  and  $\sigma_8$  into almost elliptical contours in the parameter plane (c.f. appendix A)

<sup>10</sup> In our modelling we are for example not considering the finite bin width in our measurement of  $\hat{\xi}$ .

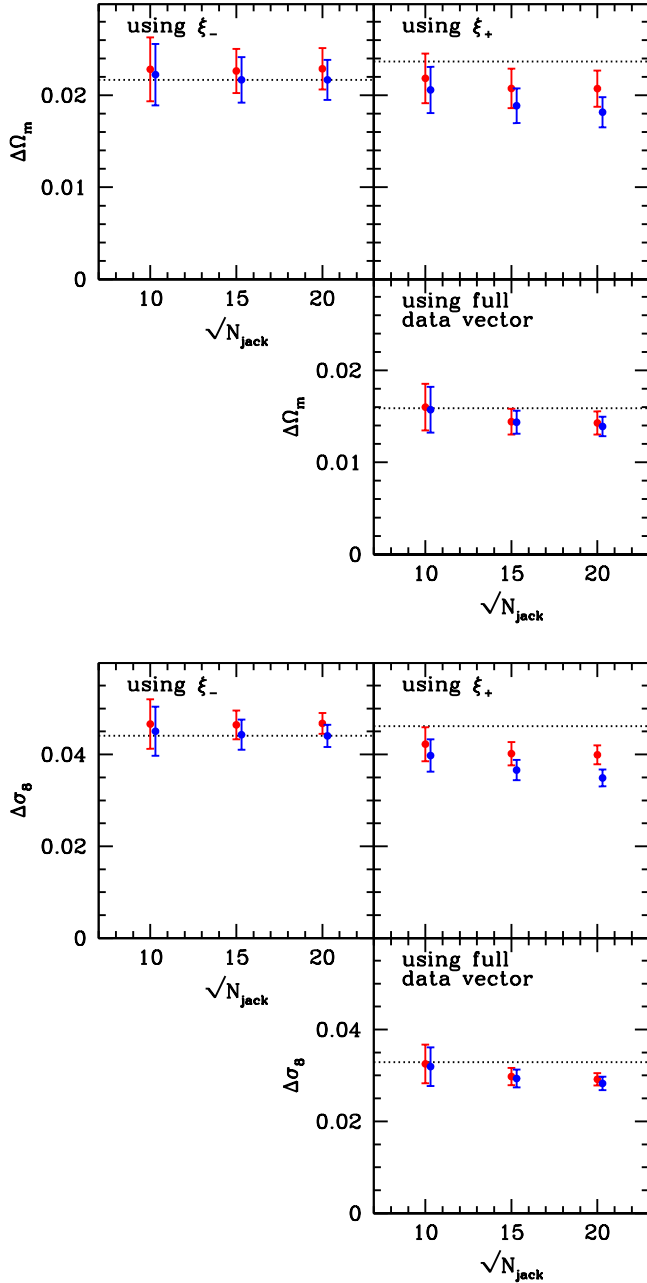


**Figure 9.** Mean width of the  $1\sigma$  uncertainty on  $\Omega_m$  and  $\sigma_8$  using pair-jackknife (blue) and galaxy-jackknife (red). The errorbars show the standard deviation of the mean, as estimated from the 50 best fit values. The black dotted line indicates the mean width of the confidence intervals when the true covariance is used in each mock catalog.

Hence, the answer to what is the best estimation scheme and how well it can reproduce the true errorbars on cosmological parameters depends on the depth of the considered survey. A shallower survey not only has a smaller source density and hence a bigger shape noise. It also has a smaller convergence power spectrum which in turn reduces the cosmic variance part of the covariance.

The procedure we presented above to investigate the

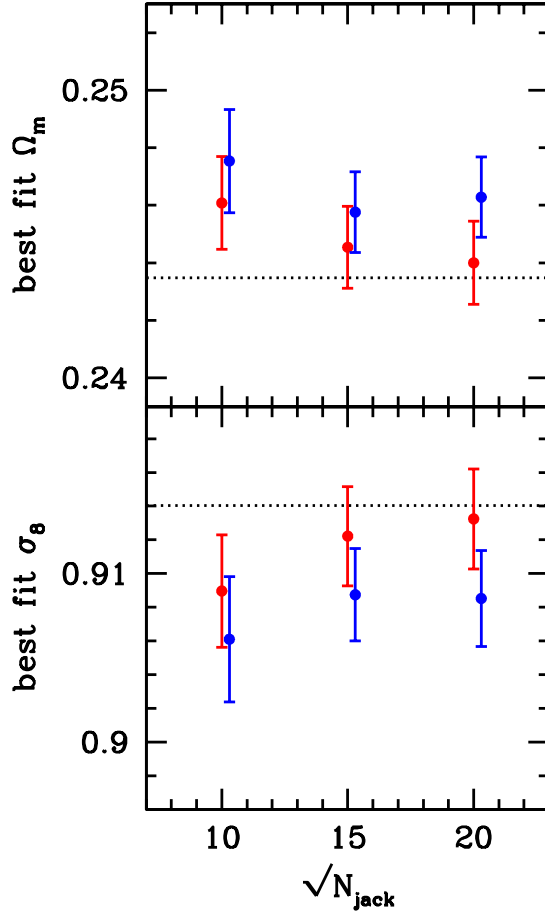


**Figure 10.** Mean best fit values of  $\Omega_m$  and  $\sigma_8$  using pair-jackknife (blue) and galaxy-jackknife (red). The errorbars show the standard deviation of the mean, as estimated from the 50 best fit values. The black dotted line indicates the mean best fit value when the true covariance is used in each mock catalog.

performance of internal covariance estimators thus has to be re-run for each survey under consideration. One can consider the log-normal model as a good model for the true covariance of our simulations for mock catalogs with an area of  $\gtrsim 1000 \text{ deg}^2$  and a simple, connected geometry. For smaller surveys the finite-area-effect should not be ignored (Sato et al. 2011; Kilbinger et al. 2013). However, these surveys can be simulated fast enough with our public code to generate a large sample of independent realisations of the mock data which provides a good sample covariance estimate of the true covariance matrix. This estimate can then be compared to an ensemble of internal covariance estimates as we have done it above.

## 5.2 Matching the procedure to DES science verification and year 5 Data

We will now present an application of our method. Our attempt is to determine the performance of internal covariance estimation for

- Dark Energy Survey science verification data (DES-SV)
- DES year five data (DES-Y5) assuming a low source density of  $6 \text{ arcmin}^{-2}$
- DES year five data assuming a source density of  $10 \text{ arcmin}^{-2}$ .

A source density of  $10 \text{ arcmin}^{-2}$  is forecasted for the final DES data while a density of  $\sim 6 \text{ arcmin}^{-2}$  roughly corresponds to the current status of DES science verification data.

Using a mask similar to that of the science verification data of the Dark Energy Survey (DES-SV) we will simulate mock shape catalogs to see whether internal covariance estimation can be successfully applied to that data. We keep the cosmology and the shape noise dispersion as they were before. The source redshift distribution of equation 41 will be adjusted to a value of  $z_0 = 0.495$  which corresponds to a median redshift of  $z_{\text{med}} = 0.7$  and a mean redshift of  $\bar{z} = 0.745$ . We put the mean redshift into an empirical relation  $\kappa_0(z)$  provided by Hilbert et al. (2011) and arrive at a value of  $\kappa_0 \approx 0.019$  for the convergence field of this shallower survey. The source density is adjusted to  $\sim 6/\text{arcmin}^2$  which is comparable to the current density of DES-SV. It leads to an overall number of  $\sim 2.9$  million galaxies that fall into the mask.

We adjust our data vector to that used by Becker et al. (2015), i.e. for both  $\xi_+$  and  $\xi_-$  we now use 15 logarithmic bins ranging from  $\theta = 2 \text{ arcmin}$  to  $\theta = 300 \text{ arcmin}$ . We will cut the survey into 100 sub-regions which, according to equation 40, can in principle suffice to get an accuracy of  $\sim 20\%$  in parameter uncertainties. Note that this way our biggest angular scales by far exceed the diameter of our subregions. Hence, this can be considered an on-the-edge test of internal covariance estimators. A good tool to define sub-regions in an irregular survey geometry is the *kmeans* algorithm<sup>11</sup>.

To simulate Y5 data we will stick to the same set-up but increase the area of the survey to  $5000 \text{ deg}^2$  and test two different source densities as mentioned above. We will keep the shape of these simulations as a simple square. Because of the larger area we furthermore decide to split the survey into 225 sub-regions. This should give a more stable estimate of the covariance while still yielding much larger sub-regions than in the SV-case.

In figure 11 we compare the internal variance estimates to the true covariance. The latter is taken to be the log-normal model for the Y5 simulation and a sample variance computed from 1000 independent realisations for the SV simulations. As you can see, for  $\hat{\xi}_-$  the pair-jackknife now becomes the best estimator of the variance. For  $\hat{\xi}_+$  the situation is similar to what we have seen before, i.e. both schemes mostly underestimate the variance and the galaxy-jackknife is overall closer to the true variance. However, these statements only hold for the diagonal elements of the covariance matrix. A convenient way to compare the complete covariance estimates is to derive likelihood contours from them in the desired parameter space.

We carry out a likelihood analysis in the  $\Omega_m$ - $\sigma_8$  plane for the 10 simulations that have a Y5-like area and a

source density of  $6 \text{ arcmin}^{-2}$  which is the highest density currently achieved in DES science verification data (Becker et al. 2015). In figure 12 we show the likelihood contours obtained from one of the simulations when using galaxy-jackknife, pair-jackknife and the log-normal model for the covariance matrix. The contours were obtained from Monte-Carlo-Markov-Chains (150.000 steps) using the COSMOLIKE package by Eifler et al. (2014). We present the likelihood contours from the other 9 independent simulations in appendix A. As expected, jackknife estimation underestimates the uncertainties. The input cosmology lies within the  $1\text{-}\sigma$  contour in 6 of 10 simulation, when the log-normal covariance is used. It lies within the  $1\text{-}\sigma$  contour in 5 of 10 simulation, when the covariance is estimated with jackknife (either scheme).

In table 1 we show the average ratio of the volume in the  $\Omega_m$ - $\sigma_8$  plane enclosed by the  $1\sigma$ - and  $2\sigma$ -contours when using jackknife to that when using the true covariance matrix. Since the  $1\sigma$ - and  $2\sigma$ -ellipses obtained from jackknife and from the true covariance lie well on top of each other, this ratio can be considered as the fraction of the true uncertainties that is recovered by the jackknife covariance matrices. You can see from table 1 that the volume inside contours of constant likelihood in the  $\Omega_m$ - $\sigma_8$  plane estimated with galaxy-jackknife is on average  $\gtrsim 85\%$  of the true volume while the volume estimated with pair-jackknife recovers only  $\gtrsim 70\%$  of the true volume. This agrees with the impression (from figures A1 and A2) that the contours obtained with galaxy-jackknife match better to the contours obtained from the true covariance. Note also, that the ellipses obtained from pair-jackknife have in some cases a strong off-set along the degeneracy between  $\Omega_m$  and  $\sigma_8$  compared to the true covariance and the galaxy-jackknife estimates. This is probably because pair-jackknife strongly underestimates the variance of  $\hat{\xi}_{\pm}$  at large angular scales, which causes even small fluctuations at these scales to shift the contours considerably.

Finally, we want to see how well jackknife matrices recover the uncertainties perpendicular to the degeneracy between  $\Omega_m$  and  $\sigma_8$ . To do so, we consider the parameter combination

$$\Sigma_8 := \frac{\sigma_8}{0.9} \left( \frac{\Omega_m}{0.25} \right)^{0.5}. \quad (45)$$

Contours of constant  $\Sigma_8$  are roughly parallel to the degeneracy that can be seen in figures 12, A1 and A2. For each of our 10 realisations we bin our MCMC's in  $\Sigma_8$  to estimate its probability density. Table 2 displays the average ratio of the  $1\sigma$  and  $2\sigma$  uncertainties obtained from jackknife to the uncertainties obtained from the true covariance. This time, we find that galaxy-jackknife on average yields  $\sim 90\%$  of the true uncertainties while pair-jackknife yields  $\sim 85\%$ . Hence, when the degeneracy between  $\Omega_m$  and  $\sigma_8$  is broken by other probes (such as the power spectrum of temperature fluctuation in the cosmic microwave background) the performance of jackknife covariance matrices slightly improves.

Judging from the above numbers and from the contours in appendix A we deem that  $\gtrsim 85\%$  of the true uncertainties on  $\Omega_m$  and  $\sigma_8$  in a 2D cosmic shear analysis can be recovered without the use of large suits of N-body simulations or covariance models. When other probes like the CMB are used to break the degeneracy between the two parameters,

<sup>11</sup> implemented by Erin Sheldon for python, [www.github.com/esheldon/kmeans\\_radec](http://www.github.com/esheldon/kmeans_radec)

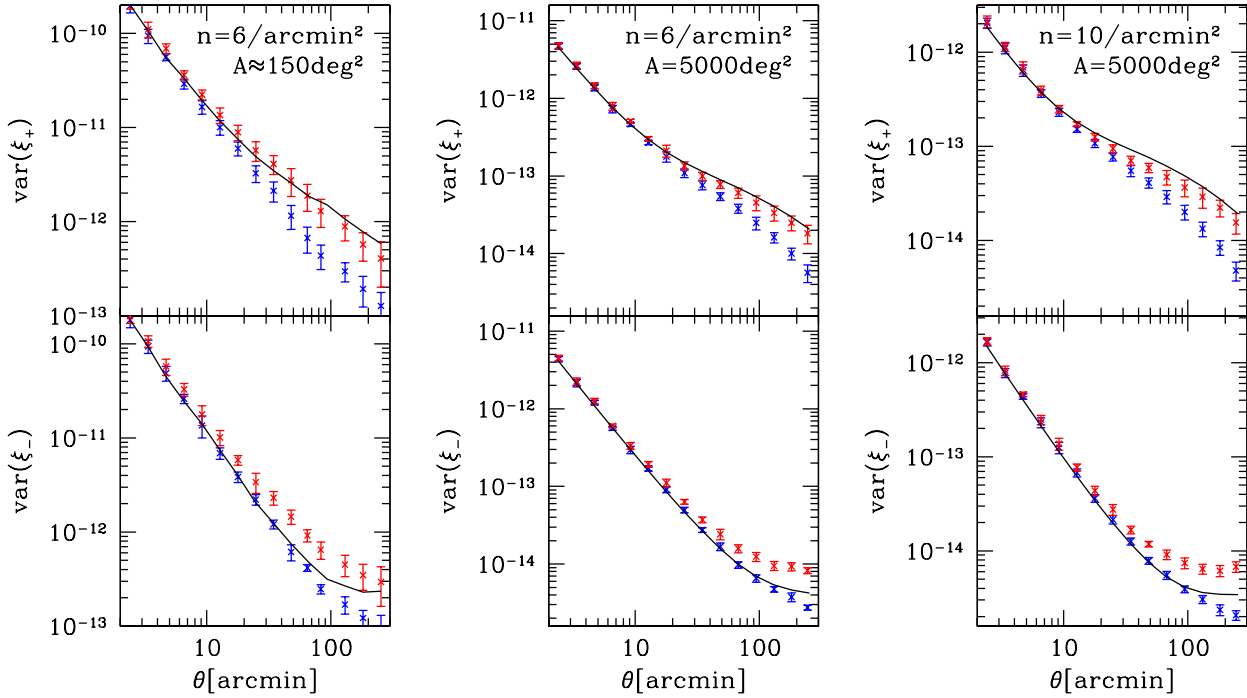


**Figure 11.** Variance estimates for DES-SV like data (left), DES-Y5 like data with a low density (middle) and with a high density (right). Red dots show the galaxy-jackknife estimates and blue dots the pair-jackknife estimates. For the Y5 case the lognormal model together with eqn. 18 was taken as a reference covariance (black lines) while for the SV case we estimated the true covariance from 1000 independent realizations of the mock data in order to account for the finite-area-effect. The errorbars indicate the standard deviation of the single estimates as obtained from 10 independent measurements.

the performance of jackknife even increases, because the deviations from the true covariance mostly take place along the direction of degeneracy between  $\Omega_m$  and  $\sigma_8$ .

## 6 CONCLUSIONS

We have explored the performance of internal covariance estimation for cosmic shear 2-pt. correlation functions. We devised two different jackknife schemes and explained in detail when these schemes underestimate the true covariance and when overestimation takes place. Furthermore, we explained why the sub-sample covariance and the bootstrap covariance yield results that are very similar to jackknife estimation of the covariance matrix. Based on the pair-jackknife scheme we have argued that the Anderson-Hartlap-Kaufman (Kaufman 1967; Hartlap et al. 2007) debiasing factor should also be applied when inverting jackknife covariance matrices. Based on empirical findings we also recommend the use of this factor for the galaxy-jackknife scheme.

We have demonstrated our findings in an exemplary study using log-normal simulations of the convergence field and the corresponding shear fields. We compared the performance of the different internal covariance estimators and found that the galaxy-bootstrap severely overestimates the covariance. This points to the fact that pairs of galaxies - and not individual galaxies - are the pieces of information in a cosmic shear survey and hence these pairs should be re-sampled. Since in the pair-scheme both bootstrap and

jackknife perform very similarly, we restricted our following analyses to the jackknife estimators.

For the investigated cases, jackknife covariance matrices could accurately reconstruct the constraints on cosmological parameters that were achieved using the true covariance matrix of our simulations. From  $\xi_-$  alone, the pair-jackknife scheme reconstructs the parameter constraints most faithfully (cf. figure 8). From  $\xi_+$  alone and when combining the two correlation functions, we find that the parameter constraints are best reconstructed by the galaxy-jackknife. This is because two systematic errors (cf. sections 4.4 and 4.5) cancel each other partly in the galaxy-scheme. The pair-jackknife suffers from only one of these systematics and hence always yields lower (absolute) values for the covariance than the galaxy-jackknife and always underestimates the (absolute) values of the true covariance matrix.

Our results can not be generalized to arbitrary surveys. Our paper is rather to be understood as demonstrating a general method for finding a good covariance estimation scheme for any particular survey. In making our simulation code public we provide our readers with a tool to re-do the presented analyses for their desired set-up. As an application example we tested jackknife estimation of the covariance for a 2D cosmic shear analysis of the Dark Energy Survey. We found that for the complete, 5-year DES survey internal covariance estimators can provide reliable parameter constraints in a 2D cosmic shear analysis. We recommend a scheme of  $\sim 15 \times 15$  jackknife re-samplings to yield a stable covariance matrix. Judging from figures 12, A1 and A2,



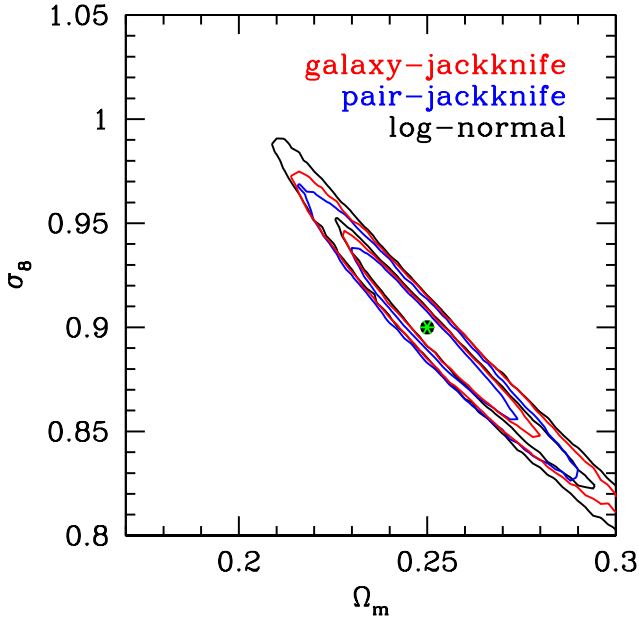


**Figure 12.**  $1\text{-}\sigma$  and  $2\text{-}\sigma$  contours in the  $\Omega_m\text{-}\sigma_8$  plane obtained from the two jackknife schemes (red and blue) and the true covariance (log-normal covariance, black). The input cosmology lies within the  $1\text{-}\sigma$  contour in 6 of 10 simulation, when the log-normal covariance is used. It lies within the  $1\text{-}\sigma$  contour in 5 of 10 simulation, when the covariance is estimated with jackknife (either scheme). In appendix A we show the contours obtained from the other simulations. The underestimation of the uncertainties by jackknife mainly takes place along the direction of the degeneracy between  $\Omega_m$  and  $\sigma_8$ .

we find as before that the likelihood contours in the  $\Omega_m\text{-}\sigma_8$  plane are best reconstructed by the galaxy-jackknife scheme, if both correlation functions  $\xi_+$  and  $\xi_-$  are combined. This way, on average  $\gtrsim 85\%$  of the true uncertainties are captured by the internally estimated covariance matrix. If the degeneracy between  $\Omega_m$  and  $\sigma_8$  is broken, this value increases to  $\sim 90\%$ . Hence, up to  $\sim 90\%$  of the true uncertainties in a 2D cosmic shear analysis can be provided from internally estimated covariance matrices.

	galaxy-jackknife	pair-jackknife
$V_{1\sigma,\text{jack}}/V_{1\sigma,\text{true}}$	$0.86 \pm 0.08$	$0.72 \pm 0.09$
$V_{2\sigma,\text{jack}}/V_{2\sigma,\text{true}}$	$0.87 \pm 0.08$	$0.74 \pm 0.09$

**Table 1.** Ratio of the volume within the  $1\sigma$  and  $2\sigma$  contours in the  $\Omega_m - \sigma_8$  plane obtained from jackknife and true covariance. The errors are given by the standard deviation of a sample of 10 independent simulations. The combined data vector of  $\xi_+$  and  $\xi_-$  was used.

	galaxy-jackknife	pair-jackknife
$\Delta\Sigma_8\ 1\sigma,\text{jack}/\Delta\Sigma_8\ 1\sigma,\text{true}$	$0.91 \pm 0.08$	$0.86 \pm 0.10$
$\Delta\Sigma_8\ 2\sigma,\text{jack}/\Delta\Sigma_8\ 2\sigma,\text{true}$	$0.90 \pm 0.08$	$0.85 \pm 0.09$

**Table 2.** Ratio of the  $1\sigma$  and  $2\sigma$  uncertainties on  $\Sigma_8 \sim \sigma_8\Omega_m^{0.5}$  obtained from jackknife and true covariance. The errors are given by the standard deviation of a sample of 10 independent simulations. Again, the combined data vector of  $\xi_+$  and  $\xi_-$  was used.

## ACKNOWLEDGMENTS

This work was supported by SFB-Transregio 33 ‘The Dark Universe’ by the Deutsche Forschungsgemeinschaft (DFG). We also acknowledge the support by the DFG Cluster of Excellence ‘Origin and Structure of the Universe’. The simulations have been carried out on the computing facilities of the Computational Center for Particle and Astrophysics (C2PAP). Part of the research was carried out at the Jet Propulsion Laboratory, California Institute of Technology, under a contract with the National Aeronautics and Space Administration.

This paper has gone through internal review by the DES collaboration. We thank David Bacon, Gary Bernstein, Stefan Hilbert, Klaus Honscheid, Benjamin Joachimi and Bhuvnesh Jain for very helpful comments and discussions during the review process.

Funding for the DES Projects has been provided by the U.S. Department of Energy, the U.S. National Science Foundation, the Ministry of Science and Education of Spain, the Science and Technology Facilities Council of the United Kingdom, the Higher Education Funding Council for England, the National Center for Supercomputing Applications at the University of Illinois at Urbana-Champaign, the Kavli Institute of Cosmological Physics at the University of Chicago, the Center for Cosmology and Astro-Particle Physics at the Ohio State University, the Mitchell Institute for Fundamental Physics and Astronomy at Texas A&M University, Financiadora de Estudos e Projetos, Fundação Carlos Chagas Filho de Amparo à Pesquisa do Estado do Rio de Janeiro, Conselho Nacional de Desenvolvimento Científico e Tecnológico and the Ministério da Ciência, Tecnologia e Inovação, the Deutsche Forschungsgemeinschaft and the Collaborating Institutions in the Dark Energy Survey. The DES data management system is supported by the National Science Foundation under Grant Number AST-1138766.

The Collaborating Institutions are Argonne National Laboratory, the University of California at Santa Cruz, the University of Cambridge, Centro de Investigaciones Energéticas, Medioambientales y Tecnológicas-Madrid, the University of Chicago, University College London, the DES-Brazil Consortium, the University of Edinburgh, the Ei-

dgenössische Technische Hochschule (ETH) Zürich, Fermi National Accelerator Laboratory, the University of Illinois at Urbana-Champaign, the Institut de Ciències de l'Espai (IEEC/CSIC), the Institut de Física d'Altes Energies, Lawrence Berkeley National Laboratory, the Ludwig-Maximilians Universität München and the associated Excellence Cluster Universe, the University of Michigan, the National Optical Astronomy Observatory, the University of Nottingham, The Ohio State University, the University of Pennsylvania, the University of Portsmouth, SLAC National Accelerator Laboratory, Stanford University, the University of Sussex, and Texas A&M University.

The DES participants from Spanish institutions are partially supported by MINECO under grants AYA2012-39559, ESP2013-48274, FPA2013-47986, and Centro de Excelencia Severo Ochoa SEV-2012-0234. Research leading to these results has received funding from the European Research Council under the European Unions Seventh Framework Programme (FP7/2007-2013) including ERC grant agreements 240672, 291329, and 306478.

## REFERENCES

- Becker M. R., Troxel M. A., MacCrann N., Krause E., Eifler T. F., Friedrich O., Nicola A., The DES Collaboration 2015, ArXiv e-prints
- Cabr e A., Fosalba P., Gazta naga E., Manera M., 2007, Monthly Notices of the Royal Astronomical Society, 381, 1347
- Cooray A., Hu W., 2001, The Astrophysical Journal, 554, 56
- Crocce M., Cabr e A., Gazta naga E., 2011, Monthly Notices of the Royal Astronomical Society, 414, 329
- de Simoni F., Sobreira F., Carnero A., Ross A. J., Camacho H. O., Rosenfeld R., Lima M., da Costa L. A. N., Maia M. A. G., 2013, Monthly Notices of the Royal Astronomical Society, 435, 3017
- Efron B., 1982, The Jackknife, the Bootstrap and other resampling plans
- Eifler T., Krause E., Schneider P., Honscheid K., 2014, Monthly Notices of the Royal Astronomical Society, 440, 1379
- Eifler T., Schneider P., Hartlap J., 2009, Astronomy & Astrophysics, 502, 721
- Flaugher B., 2005, International Journal of Modern Physics A, 20, 3121
- Hartlap J., Simon P., Schneider P., 2007, Astronomy & Astrophysics, 464, 399
- Hilbert S., Hartlap J., Schneider P., 2011, Astronomy & Astrophysics, 536, A85
- Joachimi B., Schneider P., Eifler T., 2008, Astronomy & Astrophysics, 477, 43
- Kaufman G. M., 1967, Report No. 6710, Center for Operations Research and Econometrics, Catholic University of Louvain, Heverlee, Belgium
- Kilbinger M., et al., 2013, Monthly Notices of the Royal Astronomical Society, 430, 2200
- Kilbinger M., Schneider P., 2004, Astronomy & Astrophysics, 413, 465
- Loh J. M., 2008, The Astrophysical Journal, 681, 726
- Martin S., Schneider P., Simon P., 2012, Astronomy & Astrophysics, 540, A9
- Norberg P., Baugh C. M., Gazta naga E., Croton D. J., 2009, Monthly Notices of the Royal Astronomical Society, 396, 19
- Nordman D. J., Lahiri S. N., 2007, The Indian Journal of Statistics, 69, 468
- Sato M., Takada M., Hamana T., Matsubara T., 2011, The Astrophysical Journal, 734, 76
- Schneider P., van Waerbeke L., Kilbinger M., Mellier Y., 2002, Astronomy & Astrophysics, 396, 1
- Semboloni E., van Waerbeke L., Heymans C., Hamana T., Colombi S., White M., Mellier Y., 2007, Monthly Notices of the Royal Astronomical Society, 375, L6
- Simon P., King L. J., Schneider P., 2004, Astronomy & Astrophysics, 417, 873
- Takada M., Jain B., 2009, Monthly Notices of the Royal Astronomical Society, 395, 2065
- Takahashi R., Soma S., Takada M., Kayo I., 2014, Monthly Notices of the Royal Astronomical Society, 444, 3473
- Taruya A., Takada M., Hamana T., Kayo I., Futamase T., 2002, The Astrophysical Journal, 571, 638
- Taylor A., Joachimi B., 2014, Monthly Notices of the Royal Astronomical Society, 442, 2728
- Taylor A., Joachimi B., Kitching T., 2013, Monthly Notices of the Royal Astronomical Society, 432, 1928
- The Dark Energy Survey Collaboration 2005, ArXiv Astrophysics e-prints
- Thomas S., Abdalla F., Lahav O., 2011, Monthly Notices of the Royal Astronomical Society, 412, 1669
- Vale C., White M., 2003, The Astrophysical Journal, 592, 699
- Wang Y., Brunner R. J., Dolence J. C., 2013, Monthly Notices of the Royal Astronomical Society, 432, 1961

## APPENDIX A: LIKELIHOOD CONTOURS

Figures A1 and A2 show the 1- and 2- $\sigma$  contours in the  $\Omega_m$ - $\sigma_8$  plane computed with COSMOLIKE when using galaxy-jackknife and pair-jackknife to estimate the covariance matrix (red and blue lines) and compare them to the same contours obtained from the true covariance matrix (black lines). The simulations are configured to mimic the complete, 5 year Dark Energy Survey (cf. section 5.2). The green dots represent the input cosmology of the simulations.

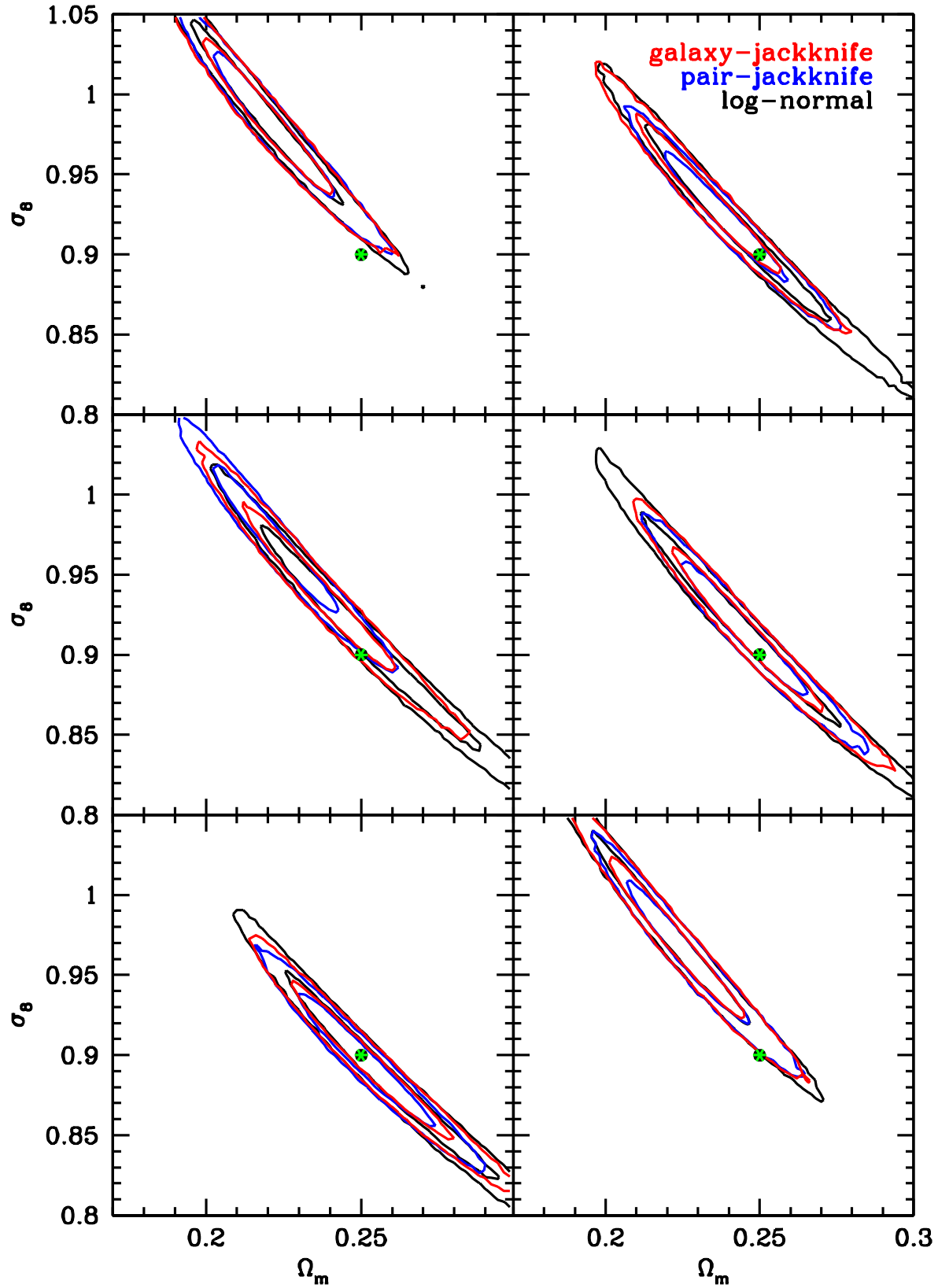


Figure A1. 1- and 2- $\sigma$  contours in the  $\Omega_m$ - $\sigma_8$  plane obtained from the first 6 simulations.

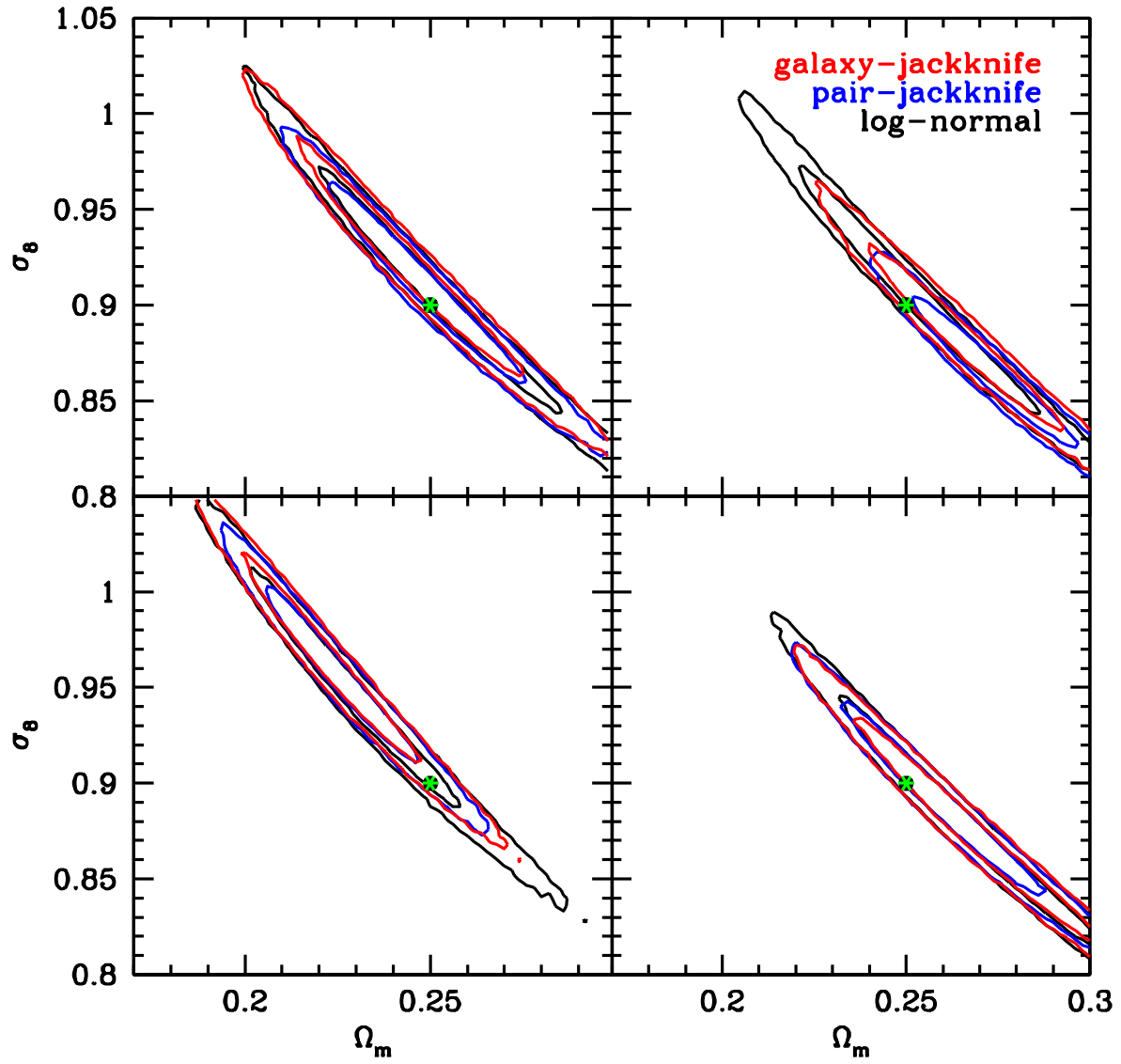


Figure A2. 1- and 2- $\sigma$  contours in the  $\Omega_m$ - $\sigma_8$  plane obtained from the remaining 4 simulations.